

<b>REPORT DOCUMENTATION PAGE</b>			<i>Form Approved</i> OMB No. 0704-0188	
Public reporting burden for this collection of information is estimated to average 1 hour per response, including the time for reviewing instructions, searching existing data sources, gathering and maintaining the data needed, and completing and reviewing the collection of information. Send comments regarding this burden estimate or any other aspect of this collection of information, including suggestions for reducing this burden, to Washington Headquarters Services, Directorate for Information Operations and Reports, 1215 Jefferson Davis Highway, Suite 1204, Arlington, VA 22202-4302, and to the Office of Management and Budget, Paperwork Reduction Project (0704-0188), Washington, DC 20503.				
<b>1. AGENCY USE ONLY (Leave blank)</b>		<b>2. REPORT DATE</b> 13.Oct.98		<b>3. REPORT TYPE AND DATES COVERED</b> THESIS
<b>4. TITLE AND SUBTITLE</b> THE EVALUATION OF MOMENTUM FLUX TO ESTIMATE EXPOSURE FROM SPRAY PAINTING OPERATIONS			<b>5. FUNDING NUMBERS</b>	
<b>6. AUTHOR(S)</b> MAJ BLAZICKO BRIAN A				
<b>7. PERFORMING ORGANIZATION NAME(S) AND ADDRESS(ES)</b> UNIVERSITY OF NORTH CAROLINA			<b>8. PERFORMING ORGANIZATION REPORT NUMBER</b>	
<b>9. SPONSORING/MONITORING AGENCY NAME(S) AND ADDRESS(ES)</b> THE DEPARTMENT OF THE AIR FORCE AFIT/CIA, BLDG 125 2950 P STREET WPAFB OH 45433			<b>10. SPONSORING/MONITORING AGENCY REPORT NUMBER</b>  98-097	
<b>11. SUPPLEMENTARY NOTES</b>				
<b>12a. DISTRIBUTION AVAILABILITY STATEMENT</b> Unlimited distribution In Accordance With AFI 35-205/AFIT Sup 1			<b>12b. DISTRIBUTION CODE</b>	
<b>13. ABSTRACT (Maximum 200 words)</b>			19990106 058	
<b>14. SUBJECT TERMS</b>			<b>15. NUMBER OF PAGES</b>	
			<b>16. PRICE CODE</b>	
<b>17. SECURITY CLASSIFICATION OF REPORT</b>	<b>18. SECURITY CLASSIFICATION OF THIS PAGE</b>	<b>19. SECURITY CLASSIFICATION OF ABSTRACT</b>	<b>20. LIMITATION OF ABSTRACT</b>	

# **The Evaluation of Momentum Flux to Estimate Exposure from Spray Painting Operations**

by

Brian A. Blazicko

A thesis submitted to the faculty of the University of North Carolina at Chapel Hill in partial fulfillment of the requirements for the degree of Masters of Science in Environmental Engineering in the Department of Environmental Sciences and Engineering, School of Public Health.

Chapel Hill

1998


Approved by:



Dr. Michael Flynn, Advisor



Dr. David Leith, Reader



Dr. Michael Symons, Reader

## ABSTRACT

**BRIAN A. BLAZICKO. The Evaluation of Momentum Flux to Estimate Exposure from Spray Painting Operations (Under the direction of Dr. MICHAEL R. FLYNN)**

Flynn developed an exposure model for spray paint mists based on the momentum flux ratio. The dimensionless momentum flux ratio is the momentum produced by the spray paint gun versus the reverse flow momentum caused by a worker. The model was tested with an anthropometric, 73 inch mechanical mannequin spraying nonvolatile oil on a flat plate in a paint booth while using a high volume, low pressure (HVLP) spray paint gun. Worker orientation to the freestream was also investigated. Momentum flux ratio, as a predictor of dimensionless concentration, produced trendlines qualitatively similar in shape and value for the HVLP and conventional spray paint guns.

Geometric similarity between this experiment and Carlton's experiment lessened the error that results from improper scaling and increased the ability to compare results between the experiments.

## ACKNOWLEDGEMENTS

I take this opportunity to sincerely thank Dr. Michael Flynn for allowing me to work under his guidance and for providing me a project so that I could complete my degree. Special thanks to Dr. David Leith and Dr. Michael Symons for giving me their time and expertise as members of my committee.

A big mahalo (thanks) to Randy Goodman and Cliff Burgess for answering my countless number of questions and for giving me their down to earth explanations and solutions. I'm grateful to you guys for allowing me to use your spray paint booth for that extended period of time to run my experiments. I hope you enjoyed the bagels!

My thanks to Jordan Kovitz and Jacky LaPointe for their friendship and for their help in the completion of this project.

Thanks Maryanne Boundy for your natural kindness and good heart and for supporting me in the Baity Lab. Thanks Pete Raynor, Jen Richmond, and the Baity Lab dudes who listened and helped me with my questions during the course of this project.

Finally, thanks Mom and Dad, brothers Rudy and Bruno, and my sister-in-law, Ginger, all of who provided me support and encouragement during my graduate work at UNC Chapel Hill.

And thank you UNC Football and Basketball teams who had outstanding seasons and made studying at this great university an enjoyable experience. God Bless.

## TABLE OF CONTENTS

LIST OF TABLES .....	v
LIST OF FIGURES .....	vi
I. INTRODUCTION .....	1
1.1 Background .....	1
1.2 Project Objectives.....	3
II. THEORY DEVELOPMENT .....	4
2.1 Exposure Model Development.....	4
2.2 Exposure Modeling with Momentum Flux.....	5
III. METHODOLOGY .....	8
3.1 Experiment Set-up.....	8
3.2 Measurement of Overspray and Transfer Efficiency .....	11
3.3 Determination of Breathing Zone Concentration.....	11
3.4 Experiment Design .....	12
IV. RESULTS.....	13
4.1 Experimental Data .....	13
4.2 Increasing Trend of the Dimensionless Concentration Group.....	15
4.3 Comparison of Experimental Data to Carlton's Converted Data.....	15
4.4 Scaling Effects.....	17
V. DISCUSSION.....	18
5.1 Experimental Data .....	18
5.2 Increasing Trend of the Dimensionless Concentration Quantity .....	18
5.3 Comparison of Experimental Data to Carlton's Converted Data.....	19
5.4 Scaling Effects.....	19
VI. CONCLUSIONS AND RECOMMENDATIONS .....	21
VII. REFERENCES .....	22
APPENDIX A: Instrument Calibration and Compressible Flow Discussion .....	24
APPENDIX B: Sample Calculations and Experimental Data.....	49

## LIST OF TABLES

Table 1. Approximate Experimental Dimensions.....	17
Table A.1. Calibration of Calibration Wind Tunnel with a 3.5 inch Orifice and Pitot Traverse Measurements .....	33
Table A.2. Calibration of Thermoanemometer with a Calibration Wind Tunnel .....	35
Table A.3. Measure of Cap and Horn Pressure of the HVLP Spray Gun.....	36
Table A.4. Calibration of HVLP Spray Gun Volumetric Airflow versus Gun Gauge Pressure Setting and Cap and Horn Pressure .....	42
Table A.5. Calibration of the Rosenau Building Paint Booth.....	43
Table A.6. HVLP Nozzle Velocity and Fg Calculation.....	51
Table A.7. Overspray and Transfer Efficiency Experiment Data .....	52
Table A.8. Dimensionless Concentration Experimental Data.....	54
Table A.9. Momentum Flux Ratio Experimental Data.....	57

## LIST OF FIGURES

Figure 1. Worker Orientation to the Freestream.....	6
Figure 2. Schematic of Air Compressor and Spray Pot.....	10
Figure 3. Functional Relationship between Dimensionless Groups with Respect to Worker Orientation.....	14
Figure 4. Comparison of HVLP and ¼-J Functional Relationships with Respect to Worker Orientation.....	16
Figure A.1. Calibration of Wind Tunnel.....	31
Figure A.2. Calibration of Calibration Wind Tunnel using a 3.5 inch Sharp-Edged Orifice and a Pitot Tube.....	32
Figure A.3. Calibration of Alnor Thermal Anemometer.....	34
Figure A.4. Calibration of the DeVilbiss HVLP Spray Gun Volumetric Air Flowrate Based on Gun Gauge Pressure.....	37
Figure A.5. Calibration of the DeVilbiss HVLP Spray Gun Volumetric Air Flowrate based on Total Horn and Cap Pressure.....	38
Figure A.6. Calibration of DeVilbiss HVLP Spray Gun Total Cap and Horn Pressure based on Gun Gauge Pressure.....	39
Figure A.7. Calibration of DeVilbiss HVLP Spray Gun Cap Pressure based on Gun Gauge Pressure.....	40
Figure A.8. Calibration of DeVilbiss Spray Gun Horn Pressure based on Gun Gauge Pressure.....	41
Figure A.9. Schematic of Workroom Obstacles—Mannequin Oriented in the 90-degree Position.....	46
Figure A.10. Schematic of Workroom Obstacles—Mannequin Oriented in the 180-degree Position.....	47

Figure A.11. Converging Nozzle Diagram.....	48
Figure A.12. Mannequin at 90 Degree Orientation to the Freestream.....	59
Figure A.13. Mannequin at 180 Degree Orientation to the Freestream.....	60

## **I. INTRODUCTION**

### **1.1 Background**

The idea that employees will be provided a work environment free from recognized hazards is the crux of the General Duty clause of the Occupational Safety and Health Act (OSHA) of 1970.<sup>(1)</sup> Prior to the establishment of OSHA, and since then, the discipline of industrial hygiene has sought to recognize, evaluate, and control workplace hazards. Many of the hazards in today's work environments have been evaluated through air sampling, toxicology, epidemiology, and biological markers of exposure. Guidelines of acceptable exposure to materials are published by the American Conference of Governmental Industrial Hygienists (ACGIH) and appear as Threshold Limit Values (TLVs) and Biological Exposure Indices (BEIs).<sup>(2)</sup> Many methods are available to the industrial hygienist to control workplace hazards and to protect the employee. Control methods include: (1) those outlined in the Industrial Ventilation Manual, (2) substitution of the hazardous material if possible, and (3) respiratory protection as a last option if other controls are not viable.<sup>(3)</sup>

An option for workplace health evaluation is exposure modeling. When the determinants of exposure are recognized, a model can be developed to predict exposure as a function of the determinants. Models can be developed conceptually by identifying the general relationship between generation and transport processes leading to the exposure within the framework of the industrial operation.<sup>(4)</sup> Further refinement can occur with dimensional analysis, which groups variables into dimensionless parameters that are fewer in number than the original variables.<sup>(5)</sup> The resultant model is an "empirical-conceptual model."

An exposure model for conventional spray gun operations was developed by Carlton. The model related the breathing zone concentration and overspray generation rate to the liquid properties of the spray paint, spray paint gun nozzle pressure, freestream velocity, and the orientation of the worker in a cross-draft wind tunnel (or Carlton number).<sup>(4)</sup> Field tests of the model confirmed its ability to predict the exposures of workers using conventional spray paint guns.<sup>(4)</sup>

Carlton's exposure model was applied to the DeVilbiss high volume, low pressure (HVLP) spray painting gun operations by McKernan<sup>(6)</sup> and Dunn<sup>(7)</sup>. They discovered that the trendlines of the two spray painting systems looked similar, but occurred over different ranges of Carlton numbers. Therefore, the motivation for this project is to understand what factors may be causing this difference, and how the difference may be minimized.

The first factor to consider is whether McKernan and Dunn applied the laws of similarity to scale their experiments from Carlton's experiment. One of the criteria of similarity, specifically geometric similarity, requires all body dimensions in all three coordinates to have the same linear-scale ratio between the model and prototype.<sup>(8)</sup> Also, all angles, flow directions, orientations between the model and prototype with respect to the surroundings must be identical.<sup>(8)</sup> Carlton tested his exposure model in the Baity Building wind tunnel using a child mannequin. McKernan and Dunn tested the HVLP spray paint gun in the same wind tunnel and in the larger Rosenau Building paint booth using a truncated, adult mannequin. For example, the ratio of mannequin area (height x breadth) to the wind tunnel area was very different for McKernan and Dunn when compared to Carlton's work. Therefore, better comparisons can be made between experiments when geometric similarity is maintained.

The second factor to consider is the design difference between the two spray paint guns. An HVLP spray paint gun uses a high air-to-liquid flow ratio to atomize the paint and operates at a maximum air cap pressure of 10 pounds per square inch gauge (psig).<sup>(9)</sup> A conventional spray paint gun uses high pressure to atomize the paint and operates at a cap pressure of 50 to 60 psig. The resultant exit velocity is sonic for the conventional spray paint gun and subsonic for the HVLP.

Carlton's exposure model assumed sonic conditions at the nozzle. The conventional spray paint gun meets this criterion, but not the HVLP. The jet exit velocity is an important criteria since Kim<sup>(10)</sup> determined that the momentum from a nozzle, which is the mass flowrate times its velocity, affects the reverse flow region downwind of the mannequin in a freestream, and thus the concentration of contaminant in the breathing zone. Kim developed the momentum flux ratio, which is the momentum from the spray paint gun divided by the momentum of the reverse flow region. Based on Kim's work, the momentum flux ratio takes into account the different exit velocities of the spray paint guns and could be used to predict the exposure of a worker. If the Carlton number is replaced with the momentum flux to predict exposure, this new model assumes that the liquid properties have little influence on contaminant transport to the breathing zone. Conversion of the data from Carlton, McKernan, and Dunn into the momentum flux ratio gives a preliminary indication as a more consistent predictor of exposure than the Carlton number.

## **1.2 Project Objectives**

This project tests the hypothesis that the momentum flux ratio may predict the dimensionless breathing zone concentration with one trend line for both the conventional

and HVLP spray paint guns. An anthropometric mannequin and an emphasis on geometric similarity were used during the experimental runs in the 90° and 180° orientations.

## II. THEORY DEVELOPMENT

### 2.1 Exposure Model Development

Carlton<sup>(4)</sup> developed an empirical-conceptual model to predict the breathing zone concentration of paint mists during spray painting tasks. He introduced the following three sequential processes common to all spraying tasks and related to exposures: (1) droplet formation, (2) droplet transfer, and (3) droplet transport/evaporation.

In a spray paint gun, the air stream discharged through the annulus surrounding the liquid stream causes droplet formation by exerting shear forces on the liquid. The two streams mix away from the nozzle in a process called twin-fluid atomization.<sup>(11)</sup> Additional air through the two horns attached to the cap regulates the desired spray pattern. The resulting mist can contain particles less than 50  $\mu\text{m}$  in mass median diameter (MMD) that can be easily inhaled.<sup>(11)</sup> Carlton determined that nozzle pressure ( $p_n$ ), liquid paint viscosity( $\mu_l$ ), and the ratio of air to liquid mass flow rates ( $m_a/m_l$ ) are salient parameters of droplet formation.<sup>(4)</sup>

Droplet transfer occurs after the droplet is formed at the nozzle. The air jets of the spray paint gun impart a momentum to the droplets. The droplets are either transferred to the object being painted or they become the overspray observed during spray painting. Droplets with sufficient size and momentum will impact the object; otherwise, the droplets will follow the airstreams created by the painting operation. Carlton determined that nozzle pressure ( $p_n$ ) and overspray ( $m_o$ ) affect droplet transfer.<sup>(4)</sup>

Droplet transport and evaporation affects the overspray from the painting operation. Transport may involve controlling the overspray with exhaust ventilation, which is found in a properly designed paint booth. Evaporation of small droplets and the solvents used in the paint may also occur. Both processes may cause exposure to the employee. The orientation of the worker, as shown in Figure 1, may increase/decrease the worker's exposure. Carlton used the freestream velocity ( $U$ ), worker orientation ( $90^\circ$  or  $180^\circ$  to the incoming freestream), breathing zone concentration ( $C$ ), and the height ( $H$ ) and breadth ( $B$ ) of the worker for his exposure model.<sup>(4)</sup>

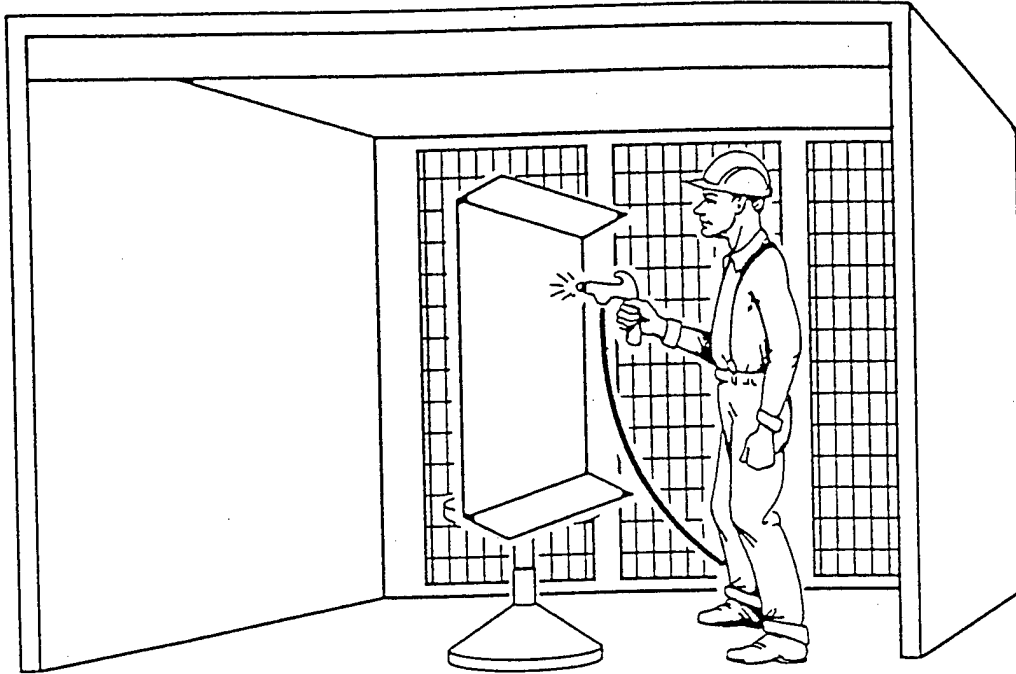
Using dimensional analysis, Carlton developed the following model to relate exposure and the operation of a conventional spray gun:

$$\frac{CHUD}{m_o} = \Phi \left[ \frac{m_a}{m_l}, \frac{p_n H}{\mu_l U}, \text{orientation} \right] \quad (1)$$

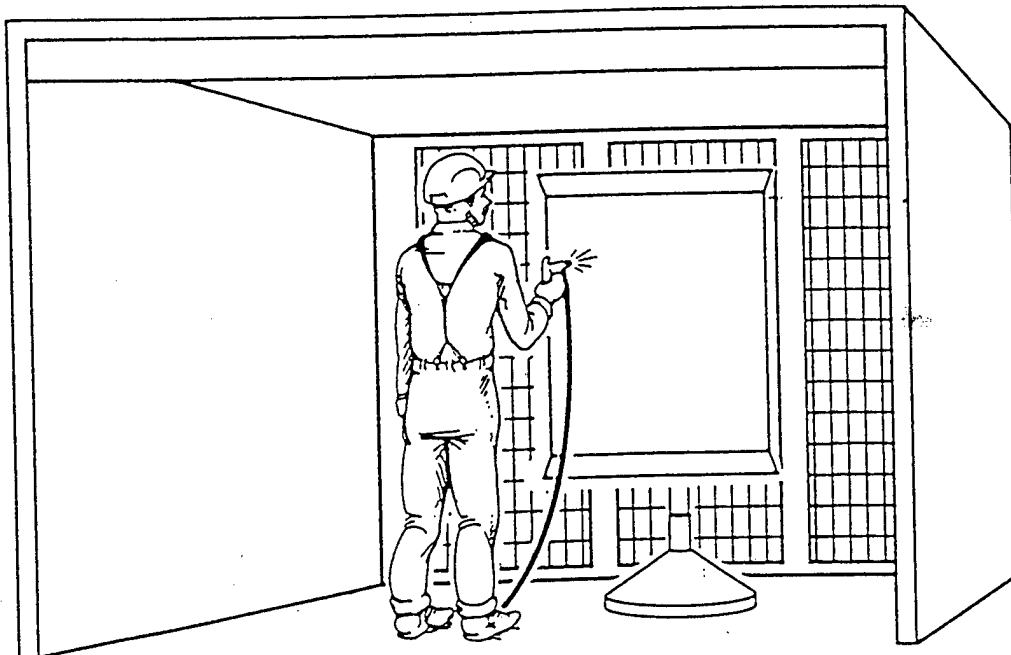
When the dimensionless concentration,  $CHUD/m_o$ , is plotted as a function of the Carlton number,  $p_n H/\mu_l U$ , the dimensionless concentration varied as a complex function of the dimensionless liquid properties in both the  $90^\circ$  or  $180^\circ$  worker orientation to the freestream.

## 2.2 Exposure Modeling with Momentum Flux

Air exiting the conventional and HVLP spray paint guns with sonic and subsonic exiting velocities, respectively, impart momentum to the freestream velocity field. Liquid droplets formed from atomization have insignificant momentum as compared to the air; thus, subsequent discussion of momentum refers only to the air momentum. The momentum imparted from the spray paint gun is referred to as  $F_g$ .



**90° ORIENTATION**



**180° ORIENTATION**

Figure 1: Worker Orientation to the Freestream<sup>(4)</sup>

Reverse flow occurs downstream from a worker as the freestream loses its kinetic energy to the frictional forces of the immediate boundary layer of the worker. The reverse flow is related to the exposure of a worker.<sup>(12)</sup> The momentum of the reverse flow caused by the worker is referred to as  $F_m$ .

Kim<sup>(10)</sup> determined that the ratio of the momentum flux of a nozzle to the reverse flow momentum is related to the exposure of the worker. Incorporating this knowledge into equation (1), the following relationship is developed:

$$\frac{CHUD}{m_o} = \Phi \left[ \frac{F_g}{F_m}, \text{orientation} \right] \quad (2)$$

The breathing zone concentration is now a function of the momentum flux ratio.

The momentum flux ratio can be written as:

$$\frac{F_g}{F_m} = \frac{\rho_n A_n V_n^2 + (p_n - p_a) A_n}{\rho_a H D U^2} \quad (3)$$

where  $\rho$  is the density of the gas at the nozzle exit (n) or ambient (a),  $A_n$  is the nozzle area of the cap and horn,  $V_n$  is the air exit velocity at the nozzle,  $p$  is the pressure at the nozzle exit or ambient,  $H$  is the worker height,  $D$  is the worker diameter (breadth), and  $U$  is the velocity of the freestream. The numerator in Equation (3) is the momentum flux from the spray paint gun and  $\rho_a H D U^2$  is the momentum flow through the projected area of the worker. The term  $(p_n - p_a) A_n$  adjusts for pressure difference between the cap and ambient air the conventional spray paint gun. This term is negligible for subsonic flows.

The  $F_g/F_m$  ratio is an index that can inform the researcher whether the gun momentum or the vortex shedding effect dominates the flow regime around the spray painter. By understanding which momentum flux dominates during a painting process, an exposure prediction can be made.

### III. METHODOLOGY

#### 3.1 Experiment Set-up

This project followed the objectives of Section 1.2 so that data obtained in this experiment could be compared to data obtained by Carlton. The ratio of the adult mannequin's 14 inch chest diameter to the child mannequin's 8 inch chest diameter (used in Carlton's experiments) is 1.75. Therefore, the new plate used in this project is 42 inches wide and 63 inches in height. Carlton used a plate 24 inches by 36 inches. The adult mannequin is 73 inches in height and the child mannequin is 41 inches in height.

The adult mannequin was positioned in the Rosenau Building paint booth in the 90° and 180° orientations with the DeVilbiss HVLP spray paint gun in the mannequin's right hand. The spray gun cap was positioned 8 inches from the target and 51 inches off the floor. The sampling cassette was located at approximately 25 inches from the target. In the 180° orientation, the mannequin was centered in the paint booth with its right arm positioned nearly mid-way on the target causing the target to be positioned slightly to the right if one were looking into the tunnel of the booth (see Figure A.10, Appendix A). In the 90° orientation, the mannequin remained the same distance from the paint booth's filter banks and the target, and the right hand was upstream of the paint booth. The target was 19 inches from the right wall if one were looking into the tunnel of the booth (see Figure A.9, Appendix A).

The paint booth is 75 inches wide, 87 inches high, and 164 inches deep as measured from the flange side of the booth entrance. The paint booth is located in the machine shop in the basement of Rosenau Building which contains many machining tools and cabinets that can disrupt the flow of air to the entrance to the booth (see Figure A.9, Appendix A). One side of the paint booth has a flange attached to the entrance to enhance a uniform velocity profile and reduce entrance effects. The flowrate is adjusted by varying the distance between the fan and the motor (see Appendix A.4). The velocity profile was measured by a calibrated Alnor thermal anemometer (see Appendix A.2) using either a 12 or 16 point grid across the face of the paint booth (see Appendix A.4).

A Speedaire 5 horsepower air compressor mounted on a large air reservoir tank provided the requirements of the HVLP spray painting system as shown in Figure 2. The compressor delivered a constant 90 psig to the DeVilbiss galvanized spray pot. The first regulator on the spray pot bled air into the pot to pressure feed the liquid to the spray paint gun and was maintained at 10 psig during experiment runs. The second regulator controlled the pressure of the air to the spray paint gun and is referred to as the gun gauge pressure. The DeVilbiss MSV-533-4-FF HVLP spray paint gun was used throughout this project. It has a 33A air cap designed to operate at 10 psig at the cap when the gun inlet pressure is 50 psig. The HVLP spray paint gun has an air adjustment knob to regulate the mass of air through the nozzles and to select the desired fan pattern for paint application. A second knob controls the mass flow of the liquid paint. Calibration of the HVLP can be found in Appendix A.3. To be consistent with the work of prior researchers, the HVLP spray paint gun control knobs were both set to two turns from closed. Inland Vacuum Industries 99

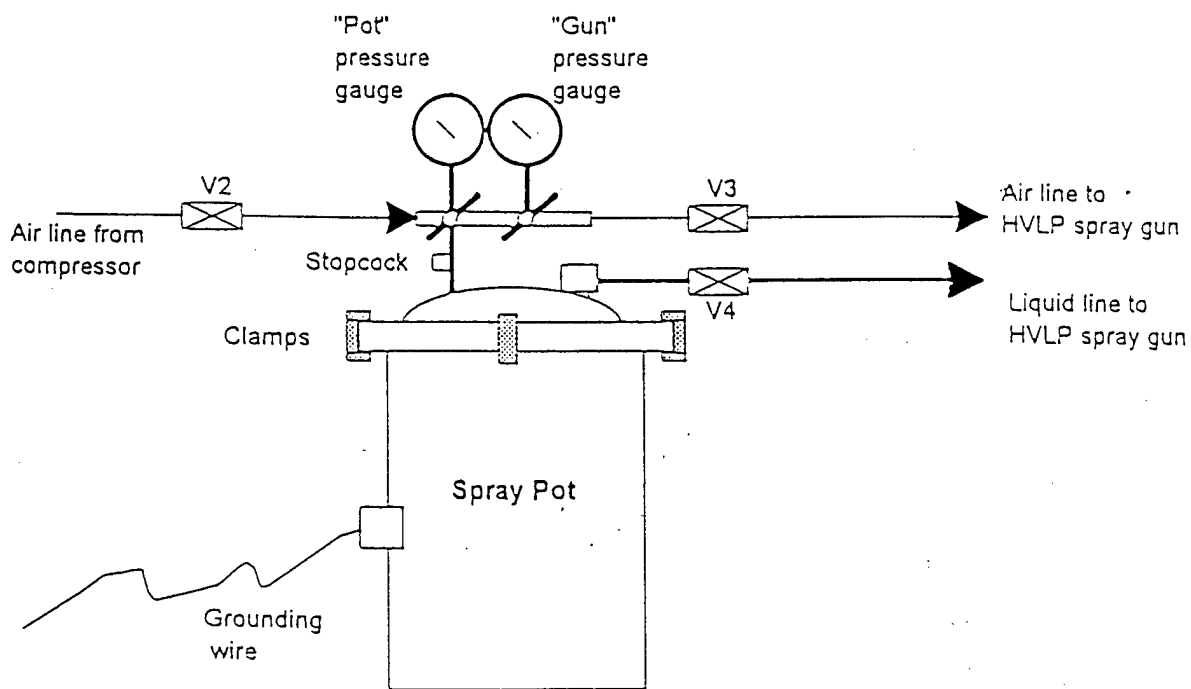
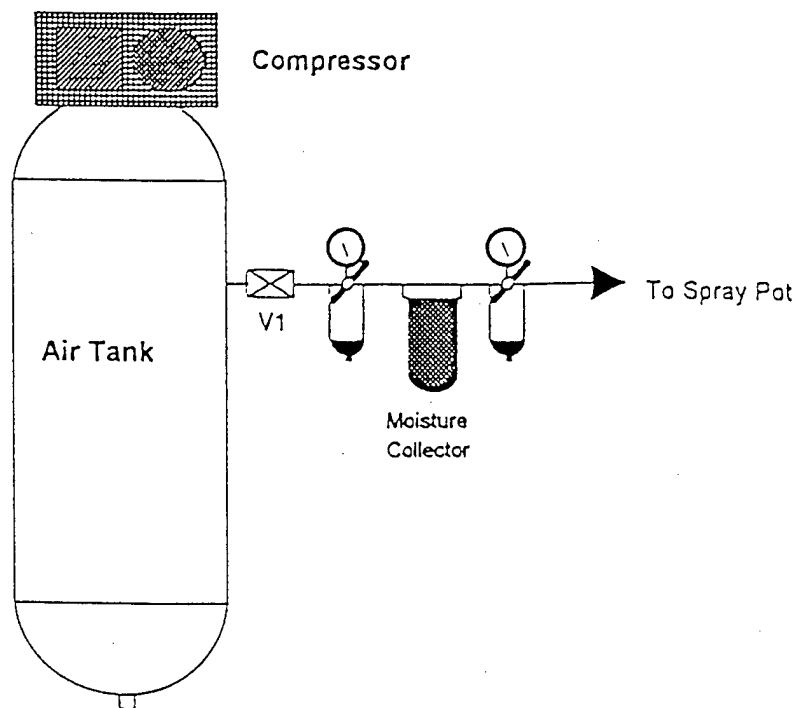


Figure 2: Schematic of Air Compressor and Spray Pot<sup>(7)</sup>

liquid ring pump seal fluid was used in lieu of actual paint because it has a low vapor pressure of less than 0.001 Torr (0.0000013 atm) at 25° C and no volatile components.

### **3.2 Measurement of Overspray and Transfer Efficiency**

The overspray ( $m_o$ ) and transfer efficiency was obtained in two steps. The bucket of oil that was placed into the DeVilbiss spray pot was weighed on a Mettler PM-34K Delta Range balance (accuracy  $\pm 0.1$  g) before and after each run to measure the mass of liquid sprayed. This mass was divided by the run time to obtain the liquid flow rate. A plastic gutter under the target collected all the oil that impacted its surface and a squeegee wiped the rest into the gutter. The gutter was weighted before and after each run and this weight was also divided by the run time to obtain the oil transferred rate. The overspray generation rate ( $m_o$ ) is the difference between the liquid sprayed rate and the oil transferred rate. The transfer efficiency is the ratio of the oil transferred rate to the liquid sprayed rate. Data for the runs are in Appendix A.

### **3.3 Determination of Breathing Zone Concentration**

NIOSH method 0500 for Total Particulates Not Otherwise Regulated <sup>(13)</sup> and ASTM Designation PS42-97 <sup>(14)</sup> were used to complete air sampling and analysis of all breathing zone concentrations (C). A 37 mm polyvinyl chloride filter with a 5  $\mu$ m pore size was used to collect oil overspray in the breathing zone. The number of blanks used either met or exceeded the NIOSH recommendation. SKC Universal Flow Sampling Pumps, Model 224-PCXR8, were pre and post flowrate calibrated by a Buck Calibration Unit Model M5 at a sampling rate of nearly 2 liters per minute. At least 5 pre and post calibration measurements were recorded and an average of the measurements was used.

The PVC cassettes were desiccated for several hours and equilibrated to room conditions prior to weighing on the Mettler-Toledo MT5 balance (accuracy  $\pm 0.001$  mg). After sampling, the cassettes were desiccated again prior to weighing and equilibrated to room conditions. Electrostatic charge potential on the filters was neutralized by resting the filter and tweezers on an alpha emitting neutralizer. The duration of spraying lasted long enough to capture between 0.1 to 2.0 mg; for the 180 orientation spraying lasted 30 minutes and for the 90 orientation spraying lasted from 10 to 30 minutes.

PVC filters and support discs were placed in modified 37 mm cassettes which have inlets the same size as the IOM inlet. The larger inlet allows for more representative exposure results. Also, IOM type inlets were used by prior researchers and should be used to allow for comparison of results between researchers. The modified PVC cassettes do not account for the loss of material that is deposited on the walls of the cassette and may be a source of error. The modified cassettes were attached to a collar hanger so they were centered directly below the mannequin's chin and in its breathing zone.

### **3.4 Experiment Design**

A reliable calibration curve for the velocity through the Rosenau Building paint booth can not be developed because the fan speed is adjusted with a large screw that does not lend itself to fine-tuning and reproducible data (see Appendix A.4). Since all the experimental runs took place in the Rosenau Building paint booth, one flowrate setting was targeted to help achieve various x-values to plot on the dimensionless momentum flux axis. At least 5 or more dimensionless momentum fluxes were achieved in the 90° and 180° orientations so comparisons can be made with the results of other researchers. Low momentum flux ratios were purposely avoided because there was large variability

experienced by prior researchers in those regions. Approximately 3 to 4 replicates per dimensionless momentum flux were completed.

## IV. RESULTS

### 4.1 Experimental Data

The dependence relationship of the concentration group  $\text{CHUD}/m_o$  on the momentum flux ratio,  $F_g/F_m$ , for the two worker orientations to the free stream is shown in Figure 3. Each error bar represents the 95% confidence interval representing approximately two standard deviations from the mean value. The error bar was calculated with t-tables due to the low number of replicates.<sup>(15)</sup> For the 180° orientation trendline, variability of the concentration group increased with increasing momentum flux ratio; for the 90° orientation, the greatest variability is observed at a low momentum flux ratio.

Regression analysis on Excel® yielded the equations below for the curves shown in Figure 3:

90° spray painter orientation to the free stream ( $R^2 = 0.991$ ):

$$\frac{\text{CHUD}}{m_o} = 0.0005 (F_g/F_m)^{1.8465} \quad (4)$$

180° spray painter orientation to the free stream ( $R^2 = 0.8426$ ):

$$\frac{\text{CHUD}}{m_o} = 0.000006 (F_g/F_m)^2 - 0.0002 (F_g/F_m) + 0.0052 \quad (5)$$

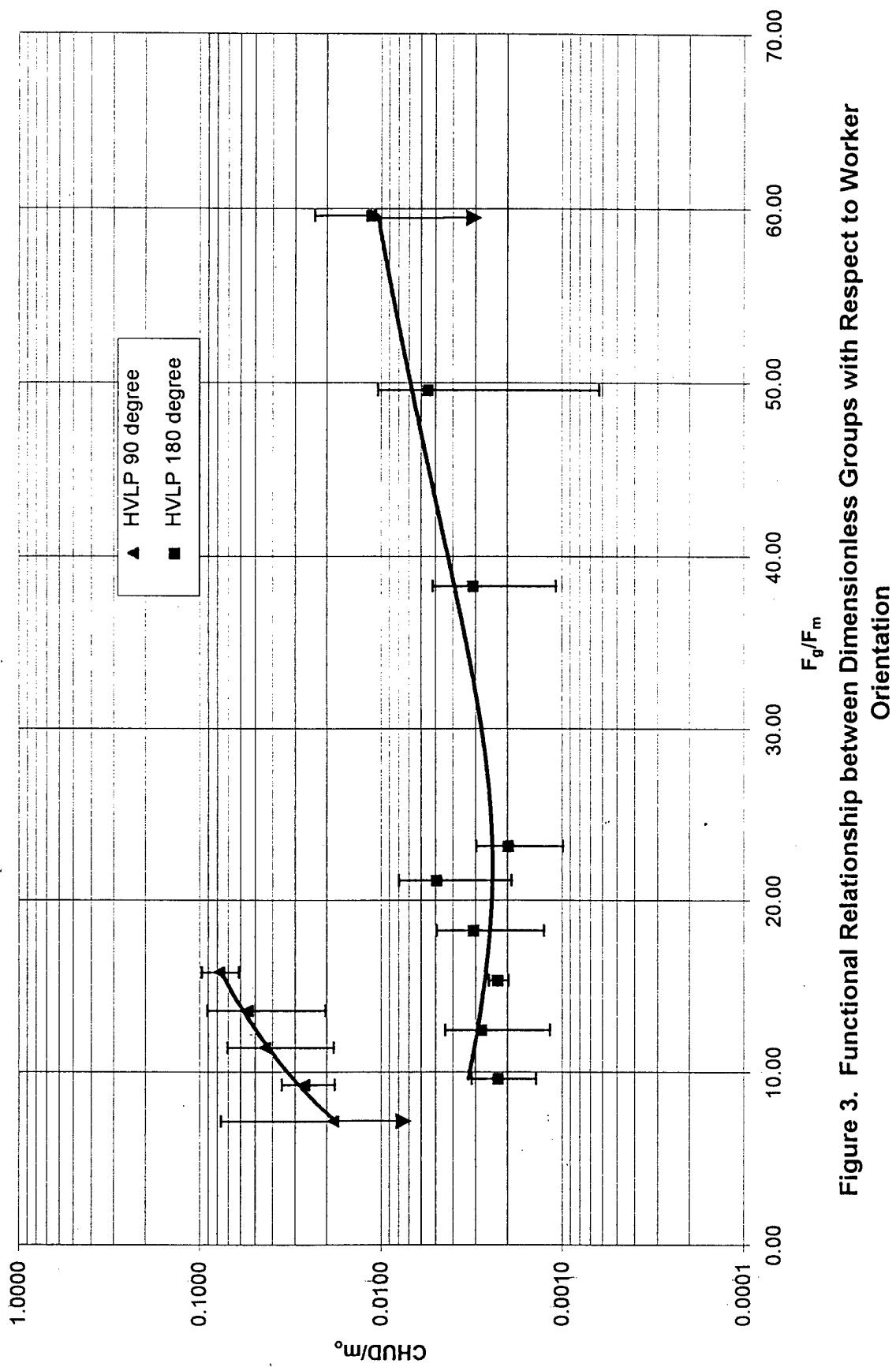


Figure 3. Functional Relationship between Dimensionless Groups with Respect to Worker Orientation

## **4.2 Increasing Trend of the Dimensionless Concentration Group**

There is a notable increase in the concentration group value as momentum flux increased in value for the 180° worker orientation. At momentum flux values of approximately 50 or greater, the variability of the concentration group increased with increasing momentum flux. The lower half of the 95% confidence interval for the concentration group with the corresponding highest momentum flux value could not be supported on the logarithmic scale, and is represented by an arrow. During the preparation of individual experimental runs, the walls adjacent to the target became saturated with oil at momentum flux ratios of 50 or greater. So much oil collected on the walls that it drained to the floor causing pools to form.

For the 90° trendline, the lower half of the 95% confidence interval for the concentration group with the corresponding lowest momentum flux value could not be supported on the logarithmic scale, and is represented by an arrow.

## **4.3 Comparison of Experimental Data to Carlton's Converted Data**

Carlton's data for the dimensionless group,  $p_n H / \mu_l U$ , was converted into appropriate momentum flux ratios. An example of the conversion process is in Appendix B. Carlton's values for the concentration group  $CHUD/m_o$  were unchanged. Figure 4 contains the trendlines for both Carlton's and this project's experimental values with one standard deviation error bars.

For the 180° worker orientation, the trendlines seem to follow the same pattern. Concentration group values from this project were consistently lower than Carlton's values by a factor of 2, when the momentum flux values are similar.

For the 90° worker orientation, the trendlines also follow the same pattern. This

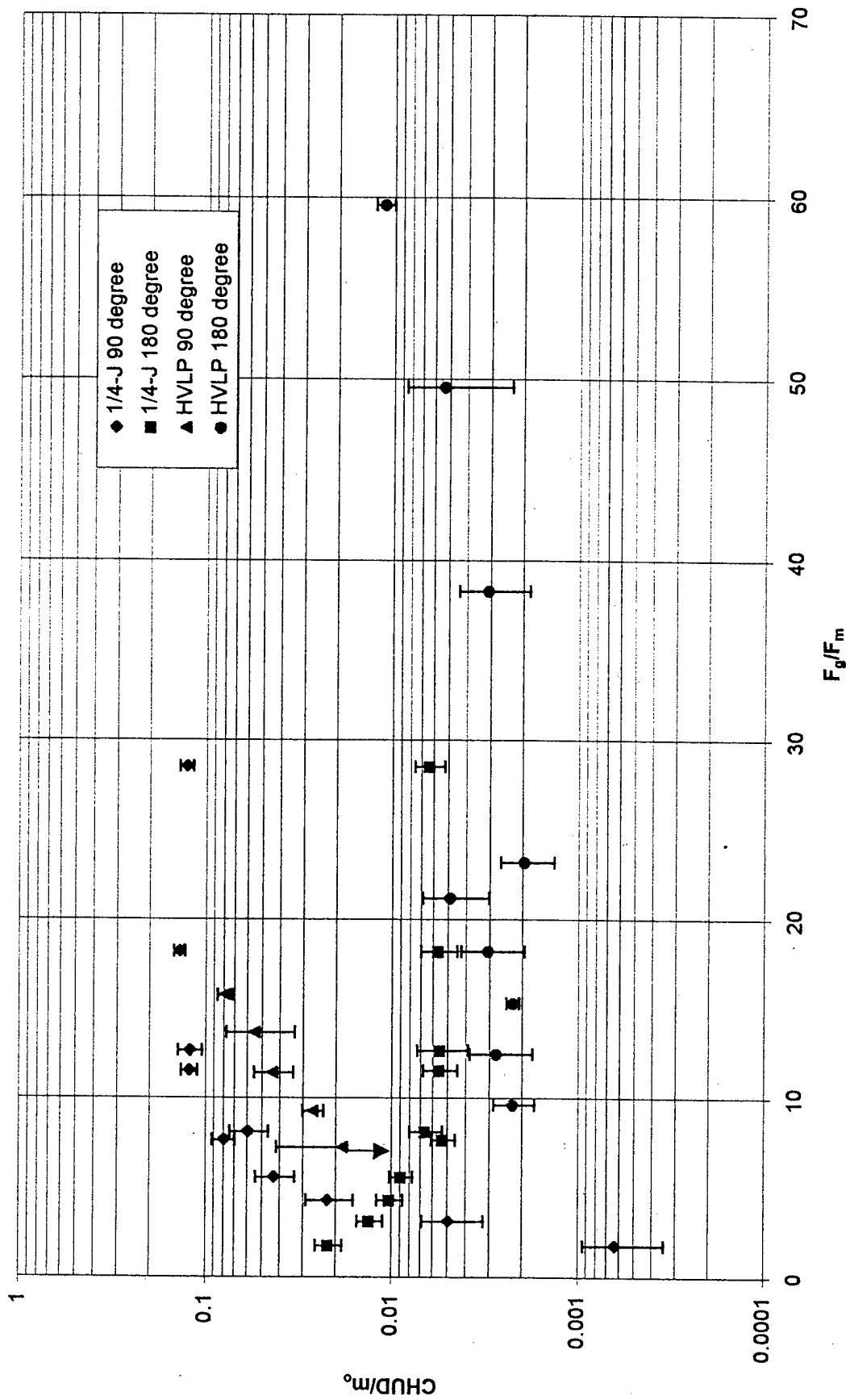


Figure 4. Comparison of HVLP and 1/4-J Functional Relationships with Respect to Worker Orientation

project's concentration group values were consistently lower than Carlton's values by a factor between 2 to 4.

#### 4.4 Scaling Effects

This project used a 6 foot, 1 inch mannequin in all of the experiments. Prior HVLP studies by McKernan<sup>(6)</sup> and Dunn<sup>(7)</sup> were all accomplished by the same adult mannequin cut off at the thighs. The reduced mannequin was able to fit in the wind tunnel; but it was never returned to its original size for experiments in the paint booth. The failure to obtain geometric similarity was thought to be a critical factor for poor correlation to Carlton's results. The length dimensions of the experiment set-up used in this project and those used in Carlton's work are presented in Table 1. As mentioned, a scaling ratio of 1.75 was employed. Note that the ratio between the mannequin arm lengths is 5.67 while other ratios are between 1 to 1.75.

Table 1. Approximate Experimental Dimensions<sup>(16)</sup>

Dimension	Conventional (1/4 J) (Inches)	HVLP (Inches)
Mannequin Height (H)	41	73
Mannequin Breadth (D)	8	14
Wind Tunnel or Paint Booth Width (Wt)	60	75
Wind Tunnel or Paint Booth Height (Ht)	60	87
Spray Paint Plate Width (Wp)	24	42
Spray Paint Plate Height (Hp)	36	63
Length of Mannequin Arm	3	17
Distance from nozzle to plate	8	8

## **V. DISCUSSION**

### **5.1 Experimental Data**

Trends in the HVLP data indicate that the operating curves will follow those for the conventional gun, but will be lower by a factor between 2 to 4. If more HVLP data is collected over a greater range of momentum flux ratios, the HVLP data is expected to follow the conventional gun trendlines.

### **5.2 Increasing Trend of the Dimensionless Concentration Group**

Variability of the dimensionless concentration group increased with increasing momentum flux ratio of the 180° trendline of Figure 4. To achieve a relatively high momentum flux ratio, a high operating cap and horn pressure combined with a low average freestream velocity were needed. It is important to note that as cap and horn pressures increase, the volumetric air flowrate increases (see Figure A.5), and the mass flowrate and the momentum of air increase. It is possible that the increase in variability was caused by the air rebounding off the flat spray piece and interfering with the oil droplets intending to impact the target. This could have increased the concentration of oil droplets in the air. Another possible cause of increased variability is the fact that the paint booth opening is smaller in this experiment than the wind tunnel opening used in Carlton's experiment. The scale ratio between the mannequins is 1.75 while the scale ratio is 1.25 between the booth and wind tunnel. Therefore, the objects in the paint booth block a greater area of the booth entrance. This means there is a smaller area for the overspray to exit through, and may have caused oil droplets to impact onto the walls. At high momentum flux operating conditions, a low freestream velocity ( $U$ ) of 45 fpm was used. At this condition, a thick mist of oil was

observed in the paint booth, transfer efficiency was lowest, and measured breathing zone concentration tended to be higher.

At low freestream velocities, little momentum is imparted to the overspray to influence its movement through the paint booth. Properly designed paint booths usually have an average freestream velocity of 100 fpm. The observance of the thick overspray emphasizes the importance of proper ventilation control to reduce exposure.

### **5.3 Comparison of Experimental Data to Carlton's Converted Data**

The use of the dimensionless momentum flux as the predictor of dimensionless concentration seems to apply to both the HVLP and the conventional spray paint guns. The curves generated in Figure 4 are similar to one another. The curves are not expected to overlap one another because geometric similarity between the projects has not been achieved.

Although all of the dimensions listed in Table 1 should have the same ratio to one another, physical limitations and cost prevented proper sizing between this project and Carlton's project. Momentum flux ratio seems to be the general factor between the two spray paint gun operations to predict similar trends of breathing zone concentration even though geometric similarity has improved since the studies by McKernan<sup>(6)</sup> and Dunn<sup>(7)</sup>.

### **5.4 Scaling Effects**

A statistical test performed by Dunn<sup>(7)</sup> indicated that there is no bias in experiments that are conducted in the paint booth versus those completed in the wind tunnel. However, using consistent scaling proportions, i.e., anthropometric mannequin versus a half mannequin, would result in a better comparison between the experiments.

The blockage ratio, or the ratio of an object's area compared to the face area of the wind tunnel or paint booth, should be similar in both experiments. Carlton's experiments in the wind tunnel had a smaller blockage ratio for both the child mannequin (.09) and the flat spray piece (.24) when compared to the blockage ratios of this experiment for the adult mannequin (.16) and spray piece (.4) in the 180° orientation. The increased concentration at higher momentum flux ratios may be caused by the higher blockage ratio. A greater blockage ratio means a lesser freestream area for the overspray to exit through. The overspray may build up and potentially form concentration gradients that could cause variability in the breathing zone samples. The oil mist was visually very dense and indicated a potentially high exposure was occurring.

Subtle differences exist between the mannequins and their use in this project and Carlton's project. Differences between the mannequins include the location of the spray paint gun and the breathing zone sample points. The child mannequin had a jet spray exiting from its stomach and a breathing zone sample cassette attached to its mouth. In contrast to the child mannequin, the adult mannequin held the HVLP spray paint gun in its right hand, which is naturally off-center to the right in the way a human would hold it. Breathing zone samples were attached to a collar hanger which hung flat against the mannequin's chest, in the same manner industrial hygiene samples are taken on humans.

The geometric dimensions that are the most influential or dominant between this experiment and Carlton's work would have to be determined empirically. Even though there is a great difference between the mannequin arm lengths, this dimension may not impact the experiments. A painstaking method of varying one dimension as all the others

are held constant, may shed light on which dimensions influence greatly on geometric similarity.

## VI. CONCLUSIONS AND RECOMMENDATIONS

The use of the momentum flux ratio as a predictor of dimensionless concentration produced trendlines that were qualitatively similar in shape and value for both the conventional and HVLP spray paint guns. The exit velocities of the two guns influence the trendlines of Figure 4 and are the important determinants in the momentum flux ratio. Momentum flux incorporates the difference in sonic and subsonic jet exit velocities of the air that is pushed through conventional and HVLP spray paint guns, respectively. Therefore, at this point in the development of modeling the exposure from spray paint gun operations, momentum flux ratio is currently the best dimensionless quantity to employ.

This conclusion infers that the liquid properties of the paint are not as important to the exposure model as the air transporting the liquid. Transfer efficiencies are indirectly included in the exposure model as overspray ( $m_o$ ), and is the only measured variable in the model related to the liquid besides the breathing zone concentration ( $C$ ).

Geometric similarity added to the success of this project. As the geometric similarity increases between experiments, dissimilarity has less of an effect on the experiment, and one can make better conclusions and inferences on experimental results.

A limited number of momentum flux ratios in the  $180^\circ$  and  $90^\circ$  orientation were investigated in this project. More data should be taken with the HVLP to expand the knowledge of the predictive nature of momentum flux on the dimensionless concentration.

## VII. REFERENCES

1. Public Law 91-596, 91<sup>st</sup> Congress, S. 2193, 29 Dec 1970.
2. American Conference of Governmental Industrial Hygienists (ACGIH). Threshold Limit Values for Chemical Substances and Physical Agents and Biological Exposure Indices. Cincinnati: ACGIH. 1997.
3. ACGIH, et al. Industrial Ventilation: A Manual of Recommended Practice, 22<sup>nd</sup> Edition. Cincinnati: American Conference of Industrial Hygienists, Inc., 1995.
4. Carlton, G. N. A Model to Estimate a Worker's Exposure to Spray Paint Mists. Ph. D. Dissertation, University of North Carolina at Chapel Hill, NC, 1996.
5. Welty, et al. Fundamentals of Momentum, Heat, and Mass Transfer, 2<sup>nd</sup> Edition. New York: John Wiley and Sons, Inc., 1976.
6. McKernan, J. L. Effect of Position and Motion on Personal Exposure in a HVLP Spray Painting Operation. Master's Thesis, University of North Carolina at Chapel Hill, NC, 1997.
7. Dunn, K. H. An Investigation of Factors Affecting the Development of an Empirical-Conceptual Model for Estimating Spray Paint Exposure in a Cross Draft Spray Booth. Master's Thesis, University of North Carolina at Chapel Hill, NC, 1997.
8. White, F. M. Fluid Mechanics, 2<sup>nd</sup> Edition. New York: McGraw-Hill. 1986.
9. Cerdoz, R. and Treuschel, J. "HVLP, the Wonder Gun." Industrial Finishing: Coatings Manufacturing and Application. Brochure. 1993.
10. Kim, T and Flynn, M. R. "The Effect of Contaminant Source Momentum on a Worker's Breathing Zone Concentration in a Uniform Freestream." American Industrial Hygiene Association. 53 (12): 757-766. 1992.
11. Kim, K. Y. and Marshall, W. R. Jr. "Drop-Size Distributions from Pneumatic Atomizers." American Institute of Chemical Engineering Journal. 17(3): 575-584. 1971.
12. George, et al. "The Impact of Boundary Layer Separation on Local Exhaust Design and Worker Exposure." Applied Occupational and Environmental Hygiene. 5(8): 501-509. 1990.
13. National Institute for Occupational Safety and Health (NIOSH). "Particulates Not Otherwise Regulated, Total: Method 0500." NIOSH Manual of Analytical Methods, 4<sup>th</sup> Edition. Cincinnati: NIOSH. 1994.

14. American Society for Testing and Materials: "ASTM Designation PS42-97" D'Arcy, J.M. Philadelphia, PA. June 19, 1997 (Memo)
15. Klienbaum, et al. Applied Regression Analysis and Other Multivariable Methods, 2<sup>nd</sup> Edition. Belmont, CA: Duxbury Press. 1988.
16. Flynn, et al. "Modeling Worker Exposure to Airborne Contaminants Generated During Compressed Air Spray Painting. Part I. Contaminant Transport and Exposure." University of North Carolina at Chapel Hill, NC. Proposed Paper for Publication.

## **APPENDIX A: Rosenau Building Paint Booth Experimental Methods and Data**

### **A.1. Calibration of Calibration Wind Tunnel with a Sharp-Edged Orifice**

A calibration wind tunnel was constructed as specified by the ACGIH Industrial Ventilation Manual and is illustrated in Figure A.1.<sup>(10)</sup> A bell shaped entry of 2.54 ft<sup>2</sup> provided uniform streamlines of entering air. The calibration wind tunnel consisted of (1) a test section where instruments are inserted for calibration, (2) a 3.5 inch diameter sharp-edged orifice attached to a manometer to measure pressure drop, (3) a pitot tube attached to a manometer to measure velocity pressure drops, (4) a damper to regulate airflow, (5) and a fan to pull air through the wind tunnel. The orifice meter was calibrated by pitot tube traverses across the 4 inch duct as specified by the ACGIH Industrial Ventilation Manual.

<sup>(10)</sup> Figure A.2 is the plot of the calibration of the wind tunnel as a function of the square root of orifice pressure drop. The relationship yielded from the plot is:

$$Q = 294.62\sqrt{h} + 6.19, \quad R^2 = 0.9994 \quad (A1)$$

where

$Q$  = Air flow through the orifice meter in cfm

$h$  = Pressure drop measured across the orifice meter in inches of water

Data used to develop the plot is in Table A.1 along with equipment specifications used with the calibration wind tunnel.

### **A.2. Calibration of Thermal Anemometer**

An Alnor Compuflow<sup>®</sup> model 8565 thermal anemometer was calibrated in the calibration wind tunnel. The thermal anemometer was inserted into the test section and the damper was adjusted to vary the pressure drop across the calibrated orifice and velocities in the test section. Nine velocities that spanned the expected working range of the thermal

anemometer were used for calibration. Figure A.3 is the plot of the thermal anemometer calibration. The calibration relationship yielded from the plot is:

$$u' = 1.0367u + 3.4675, \quad R^2 = 0.9997 \quad (A2)$$

where

$u$  = "true" velocity in the calibration wind tunnel in fpm

$u'$  = velocity measured by the Alnor thermal anemometer in fpm

The calibration equation is properly used when the Alnor thermal anemometer measurement is converted to a "true" velocity. In terms of the calibration equation, the thermal anemometer measures  $u'$  that must be converted to  $u$ . Data used to develop the calibration plot is in Table A.2.

The thermal anemometer uses the principle that the amount of heat removed by an air stream passing a heated object is related to the velocity of the air stream. Also, since the heat transfer to the air is a function of the number of molecules of air moving by a fixed monitoring point, the thermal anemometer sensing element can be calibrated as a mass flow meter.<sup>(10)</sup>

### **A.3. Calibration of the DeVilbiss HVLP Paint Spray Gun**

The DeVilbiss HVLP paint spray gun uses compressed air to push paint to the surface of the object to be painted. The air enters the spray gun from a hose connected to a compressor. As the air enters the gun, it passes over trigger and paint flow adjustments, and finally enters the nozzle section of the spray gun. At the cap of the nozzle, the air exits out the annulus surrounding the liquid nozzle and through two smaller ports. Air also exits through two ports located on both horns of the nozzle.

Pressure exerted by the compressed air on the horns and cap varied according to the pressure regulated to the spray gun. Pressure is controlled by a gauge located on the pressurized spray pot and is referred to as the gun gauge pressure. A specially fitted spray nozzle with a stem on the cap and horn was installed to determine the cap and horn pressures. When the Ashcroft pressure gauge was installed on either cap or horn stem, the other stem was capped. The spray gun air adjustment knob was opened to two turns from closed as recommended by Gatano and McKeran and the paint flow adjustment knob setting did not effect the pressure in the horn or cap.<sup>(1,2)</sup> Gun gauge pressure was taken when the trigger was depressed since pressure decreased in the compressor hose during operation. Table A.3 contains the gun gauge and its associated horn and cap pressures.

Heavy gauge plastic tubing was connected between the nozzle of the DeVilbiss HVLP spray gun and a spirometer to calibrate the HVLP. The average of four repetitions at same gun gauge pressure was completed. Figure A.4 is the volumetric air flowrate calibration of the HVLP based on gun gauge pressure. The relationship yielded from the plot is:

$$Q = 0.2439P + 2.3408, \quad R^2 = 0.9985 \quad (A3)$$

where

$Q$  = Volumetric flowrate in cfm

$P$  = gun gauge pressure in psig

Figure A.5 is the volumetric air flowrate calibration of the HVLP based on total cap and horn pressure. The relationship yielded from the plot is:

$$Q = 4.6651P^{0.4569}, \quad R^2 = 0.9991 \quad (A4)$$

where

Q = Volumetric flowrate in cfm

P = Total cap and horn pressure in psig

Figure A.6 shows how the DeVilbiss HVLP total cap and horn pressure varies with gun gauge pressure. The relationship yielded from the plot is:

$$P_{\text{cap and horn}} = 0.018P_{\text{gun}}^{1.6599}, \quad R^2 = 0.9987 \quad (\text{A5})$$

where

$P_{\text{cap and horn}}$  = Total cap and horn pressure in psig

$P_{\text{gun}}$  = Gun gauge pressure in psig

Figure A.7 shows how the DeVilbiss HVLP cap pressure varies with gun gauge pressure.

The relationship yielded from the plot is:

$$P_{\text{cap}} = 0.1736P_{\text{gun}} - 1.9006, \quad R^2 = 0.9961 \quad (\text{A6})$$

where

$P_{\text{cap}}$  = Cap pressure in psig

$P_{\text{gun}}$  = Gun gauge pressure in psig

A power function relationship for Figure A.7 yielded  $P_{\text{cap}} = 0.0104P_{\text{gun}}^{1.6657}$  with an  $R^2 = 0.9953$ . Equation (A6) has a slightly higher  $R^2$  value, and visually, a line fits the data better than the power function. Figure A.8 shows how the DeVilbiss HVLP horn pressure varies with gun gauge pressure. The relationship yielded from the plot is:

$$P_{\text{horn}} = 0.0076P_{\text{gun}}^{1.653}, \quad R^2 = 0.9993 \quad (\text{A7})$$

where

$P_{\text{horn}}$  = Horn pressure in psig

$P_{\text{gun}}$  = Gun gauge pressure in psig

Table A.4 contains the data used to plot Figures A.4 through A.8. Equations A3 through A7 were used for subsequent calculations. Note that the mass of air from the HVLP spray paint gun can be calculated by using the known density of the air at the room temperature.

#### **A.4 Calibration of Rosenau Building Paint Booth**

The Rosenau Building paint booth, located in the basement, was used to test the conditions of this project. Two wooden sheets were installed to create one wall of the paint booth. A flexible sheet of metal was attached to the wooden wall to create a curved surface reducing end effects. The paint booth ceiling was made from Plexiglas drop panels that did not extend the entire length of the paint booth. The fan motor operated at one speed and is connected to the fan by a belt and a centrifugal pulley. Adjusting the motor distance from the fan controlled the air flowrate in the paint booth. Adjusting the motor height to obtain a desired flowrate was difficult at best. Due to the odd entrance to the paint booth and other obstructions in the workshop where air was drawn from, constant turbulence was observed along the wooden board wall. Figure A.9 and A.10 illustrate the room obstacles and overhead view of the paint booth with the mannequin orientated in the 90-degree and 180-degree positions, respectively.

Velocity profiles of the 87 inch high, 75 inch wide, and 164 inch deep paint booth were completed using the preexisting, drilled holes in the wooden board made by prior researchers. Only 8 measures with the thermal anemometer were possible from this position outside the paint booth. The remaining 8 measures were made by supporting the thermal anemometer wand on a stand and hanging the meter from the ceiling supports. The meter was behind and away from the wand. The 16 velocity measurements were averaged to

determine the average flowrate of the paint booth. Since this process normally took 4 hours to accomplish, later velocity measurements were taken from only outside the drilled holes in the wooden board to reduce measurement time. This change yielded only 12 measurements and forced using an estimate for the 4 unmeasured velocity points. The thermal anemometer was acclimated for 5 minutes after being moved to a new point. The velocity was observed for 10 minutes before the mode of the point was recorded. The range of the velocity variance was recorded but is not reported. All velocity measurements reported have been corrected by the calibration equation for the thermal anemometer. Table A.5 contains various velocity profiles of the paint booth.

#### **A.5 Determination of Air Velocity Exiting a Nozzle (Compressible Flow)**

To determine the fluid velocity exiting the spray paint gun nozzle, a converging nozzle is used to model this condition as illustrated in Figure A.10. The converging nozzle is capable of sonic flow and the throat is choked. A choked throat operates at maximum mass flow when the velocity of the fluid equals the speed of sound of the fluid in the orifice. This occurs at a Mach number of 1 by the relationship:

$$Ma = \frac{V}{a} \quad (A8)$$

where  $Ma$  is the Mach number,  $V$  is the velocity of the fluid, and  $a$  is the speed of sound of the fluid. At sonic conditions in the throat, or in the orifice opening, additional mass flow occurs only when the opening is increased; constriction of the opening lessens the mass flow. By limiting the energy equation to isentropic, adiabatic flow, the characteristics of the converging, choked nozzle condition can be described in a reasonable manner. These assumptions have shown to closely approximate the actual operation of nozzles.<sup>(8)</sup>

Referring to Figure A.10, the HVLP spray paint gun uses a reservoir of compressed gas so that the reservoir pressure is equal to the stagnation pressure. Stagnation pressure is the pressure the flow would achieve if brought isentropically to rest. The HVLP pressure reservoir is reduced to lower operating pressures by a baffle in the spray paint gun. Flow is induced by decreasing the backpressure,  $p_b$ , to a pressure below  $p_o$ . A moderate drop in  $p_b$  causes the throat pressure to remain higher than the critical pressure,  $p^*$ , which is the critical pressure of a sonic throat. The flow in the nozzle is subsonic throughout, and the jet exit velocity pressure,  $p_e$ , equals  $p_b$ . The velocity is predicted by subsonic isentropic theory.<sup>(8)</sup> For this paper, the HVLP cap and horn pressure is used to predict the average exit velocity.

The conventional spray paint gun also has a large reservoir of compressed gas at the stagnation pressure. However, the conventional spray paint gun does not have a baffle in the gun to reduce the system pressure like the HVLP. Thus the conventional spray paint gun operates with a much higher stagnation pressure ( $p_o$ ) than the HVLP. The large difference between stagnation pressure and backpressure causes the pressure in the throat to reduce to  $p^*$ , but not as low as  $p_b$ , since the orifice is choked. Therefore, the throat becomes sonic ( $Ma = 1$ ) with  $p_e = p^*$ . The exit jet expands supersonically so that the jet pressure can be reduced from  $p^*$  to  $p_b$ . The velocity is predicted by supersonic isentropic theory.<sup>(8)</sup> Cap pressure measured on the ¼ J nozzle is used to predict the exit velocity.

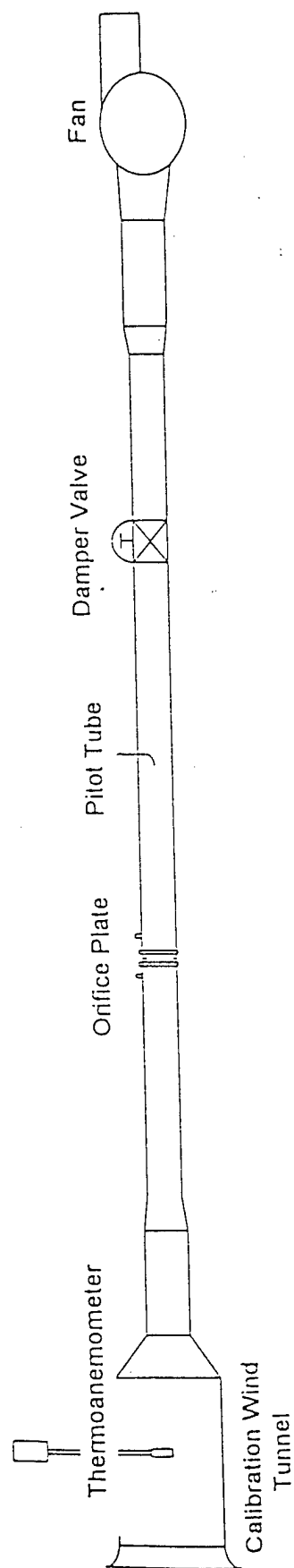


Figure A.1.: Calibration of Wind Tunnel<sup>(7)</sup>

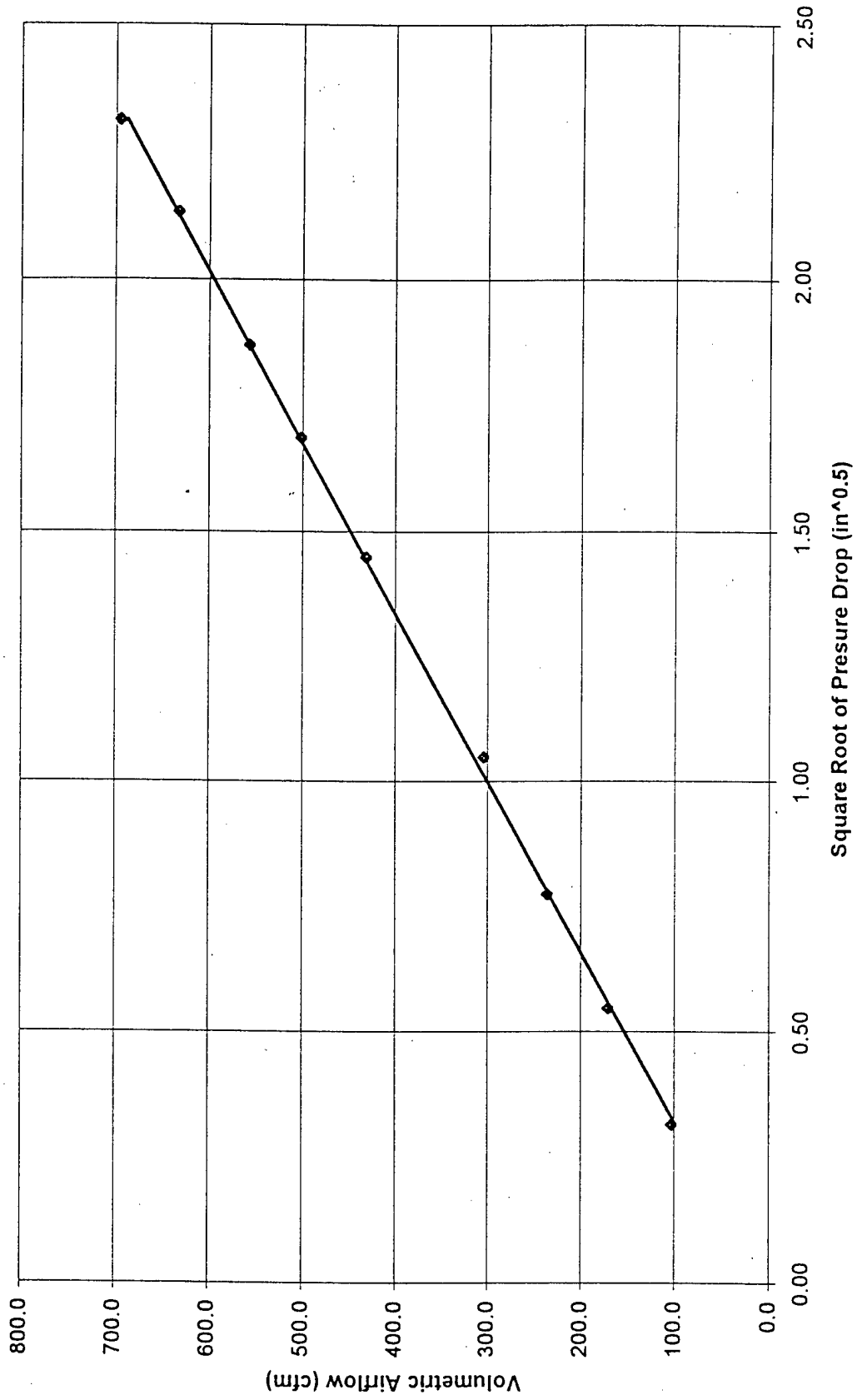


Figure A.2: Calibration of Calibration Wind Tunnel using a 3.5 inch Sharp-Edged Orifice and a Pitot Tube

Table A.1: Calibration of Calibration Wind Tunnel with a 3.5 inch Orifice and Pitot Traverse Measurements

Set up: 3.5 inch sharp edged orifice in a 4 inch round duct and pressure drop measurements with a 0-10 inch manometer  
 Pitot traverse of 4 inch round duct and velocity pressure measurements with 0-22 inches and 0-1.9 inch monometers  
 Date: 23 Jul 97; Dry Bulb: 25.6 C (78.08 F); Wet Bulb: 26 C; Rel Hum: 72%; Barometric Press: 29.67 inches Hg

Orifice Pressure Drop (inches water)		5.35(max)	4.55	3.50	2.85	2.10	1.10	0.60	0.30	0.10
Pitot Traverse Velocity Pressure (inches of water)	Top	1	3.10	1.80	1.71	1.20	0.55	0.37	0.18	0.07
		2	4.10	2.40	2.08	1.54	0.77	0.47	0.22	0.08
		3	4.20	2.70	2.20	1.62	0.82	0.48	0.26	0.10
		4	4.30	2.80	2.24	1.64	0.84	0.50	0.27	0.10
		5	4.20	2.70	2.16	1.60	0.84	0.49	0.26	0.09
		6	3.20	2.30	1.70	1.21	0.58	0.35	0.19	0.07
	Side	1	3.40	2.90	1.75	1.36	0.65	0.42	0.20	0.07
		2	4.20	3.50	2.17	1.60	0.78	0.48	0.25	0.10
		3	4.30	3.60	2.22	1.64	0.83	0.49	0.26	0.10
		4	4.30	3.60	2.25	1.66	0.84	0.49	0.27	0.10
		5	4.20	3.40	2.10	1.61	0.82	0.47	0.26	0.09
		6	3.20	2.70	1.71	1.28	0.67	0.37	0.20	0.07
Square Root of Velocity Pressure	Top	1	1.76	1.58	1.34	1.10	0.74	0.61	0.42	0.26
		2	2.02	1.82	1.55	1.24	0.88	0.69	0.47	0.28
		3	2.05	1.87	1.64	1.27	0.91	0.69	0.51	0.32
		4	2.07	1.90	1.67	1.50	0.92	0.71	0.52	0.32
		5	2.05	1.84	1.64	1.47	0.92	0.70	0.51	0.30
		6	1.79	1.64	1.52	1.30	0.76	0.59	0.44	0.26
	Side	1	1.84	1.70	1.52	1.32	0.81	0.65	0.45	0.26
		2	2.05	1.87	1.64	1.47	0.88	0.69	0.50	0.32
		3	2.07	1.90	1.64	1.49	0.91	0.70	0.51	0.32
		4	2.07	1.90	1.67	1.50	0.92	0.70	0.52	0.32
		5	2.05	1.84	1.64	1.45	0.91	0.69	0.51	0.30
		6	1.79	1.64	1.45	1.31	0.82	0.61	0.45	0.26
Ave Sqrt of VP			1.97	1.79	1.58	1.42	0.86	0.67	0.48	0.29
Velocity (fpm)			7965.2	7251.5	6384.0	5747.0	3492.9	2703.9	1956.3	1187.5
Flow Rate (cfm)			695.1	632.8	557.1	501.5	304.8	236.0	170.7	103.6

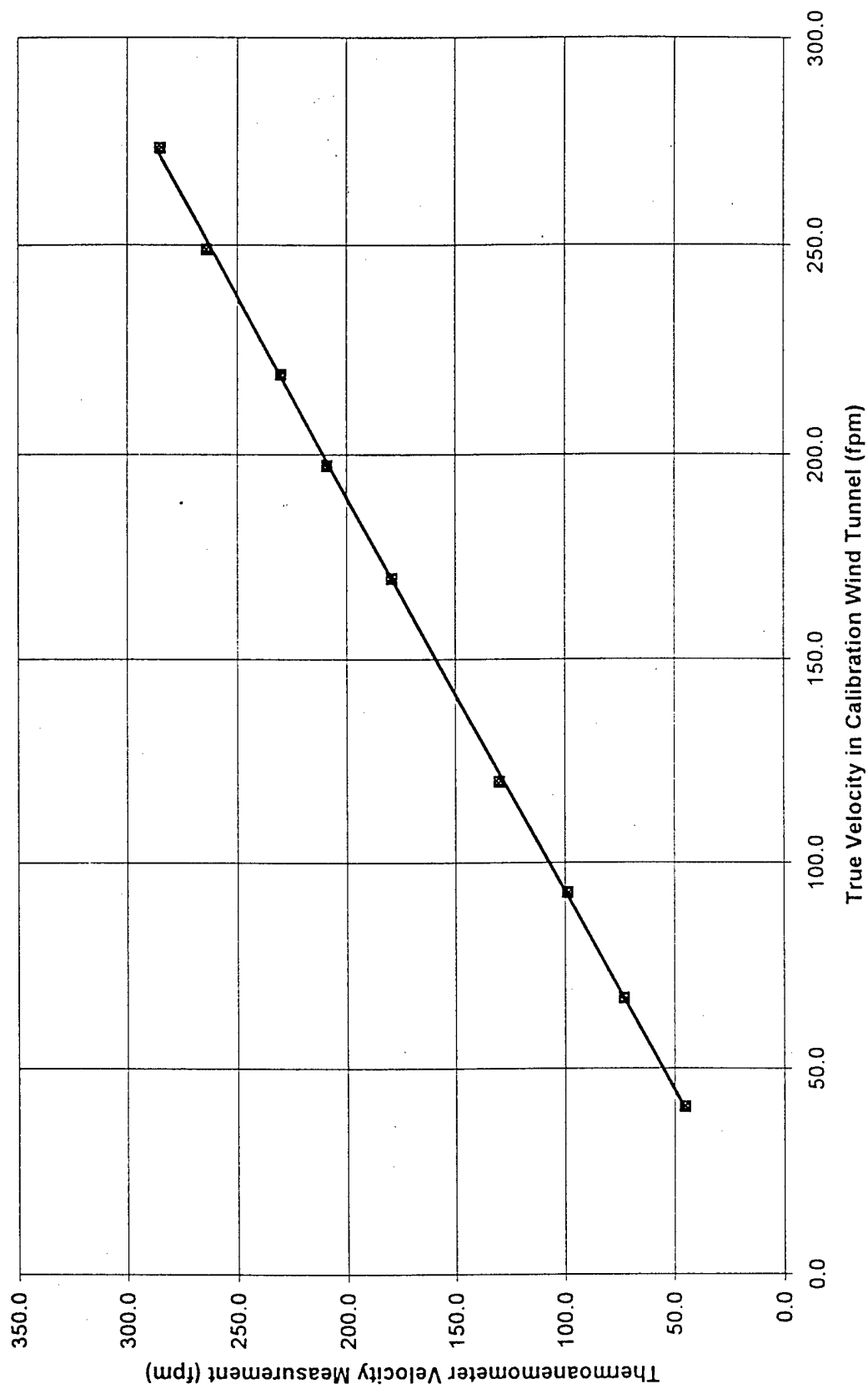


Figure A.3: Calibration of Alnor Thermal Anemometer

Table A.2: Calibration of Thermal Anemometer with a Calibration Wind Tunnel

Orifice Pressure Drop (inches water)	Square Rt Orifice Pr	Vol Air Flow CFM	Vel in Cal Tunn FPM	Thermo Ane FPM
5.35	2.31	695.1	273.7	285.0
4.55	2.13	632.8	249.1	264.0
3.50	1.87	557.1	219.3	230.0
2.85	1.69	501.5	197.4	209.0
2.10	1.45	431.2	169.8	179.0
1.10	1.05	304.8	120.0	130.0
0.60	0.77	236.0	92.9	99.0
0.30	0.55	170.7	67.2	73.0
0.10	0.32	103.6	40.8	45.0

Table A.3: Measure of Cap and Horn Pressure of the HVLP Spray Gun

The HVLP air knob was opened two turns from its closed position. Leaving the liquid control knob closed or open did not affect pressure measurements. When the HVLP trigger was depressed, the gauge pressure was adjusted to preselected settings. Unfortunately, cap pressure was measured while the horn tap was closed and horn pressure was measured when the cap tap was closed.

30 Jul 97, 1300 hrs, Baity Bay

Gun Gauge Pressure (trigger depressed) (psig)	Cap Pressure (psig)	Horn Pressure (psig)	Total Cap and Horn (psig)
16	1.00	0.75	1.75
27	2.75	1.75	4.50
38	4.50	3.00	7.50
46	6.00	4.25	10.25
53	7.50	5.50	13.00

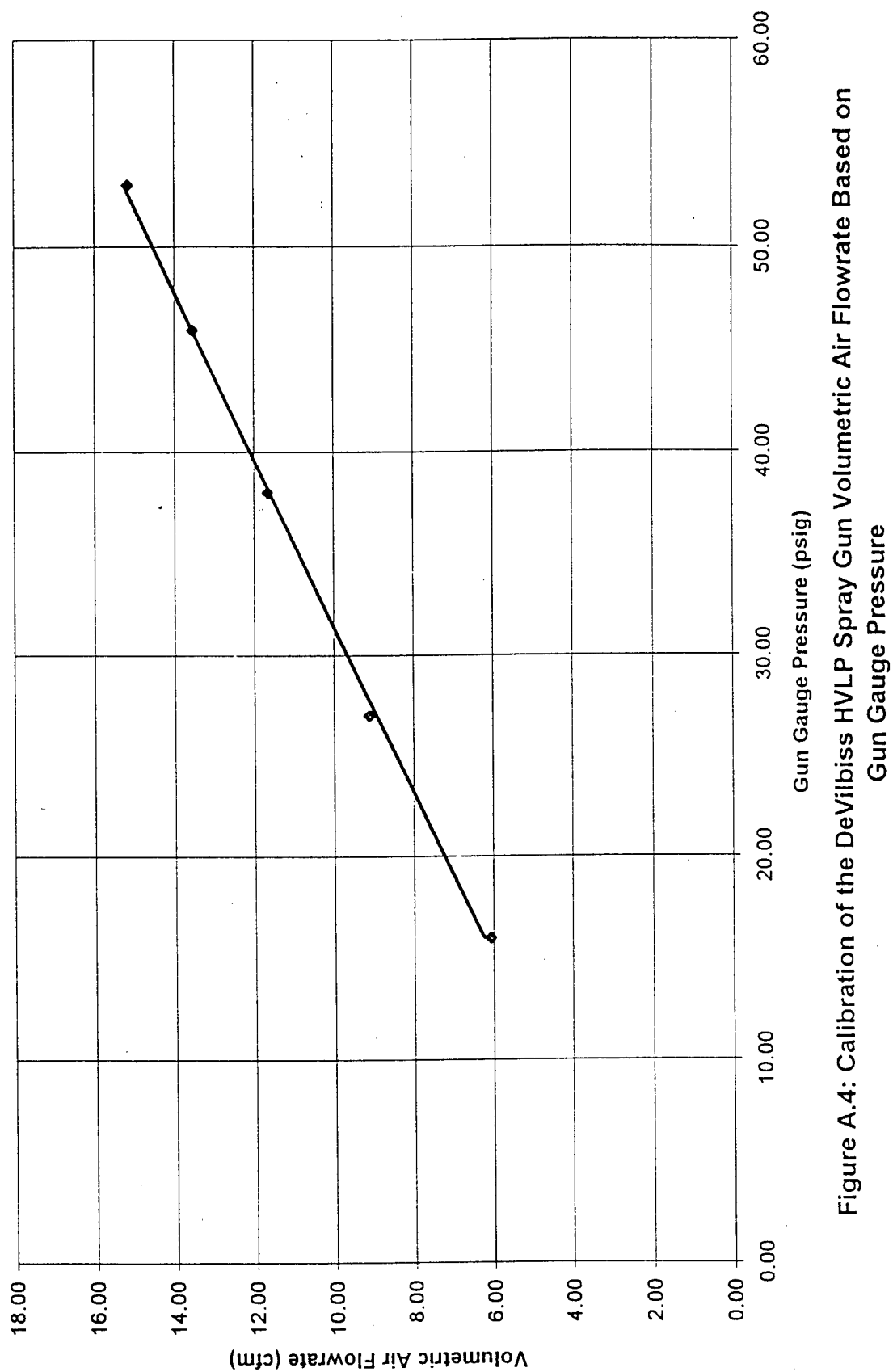


Figure A.4: Calibration of the DeVilbiss HVLP Spray Gun Volumetric Air Flowrate Based on Gun Gauge Pressure

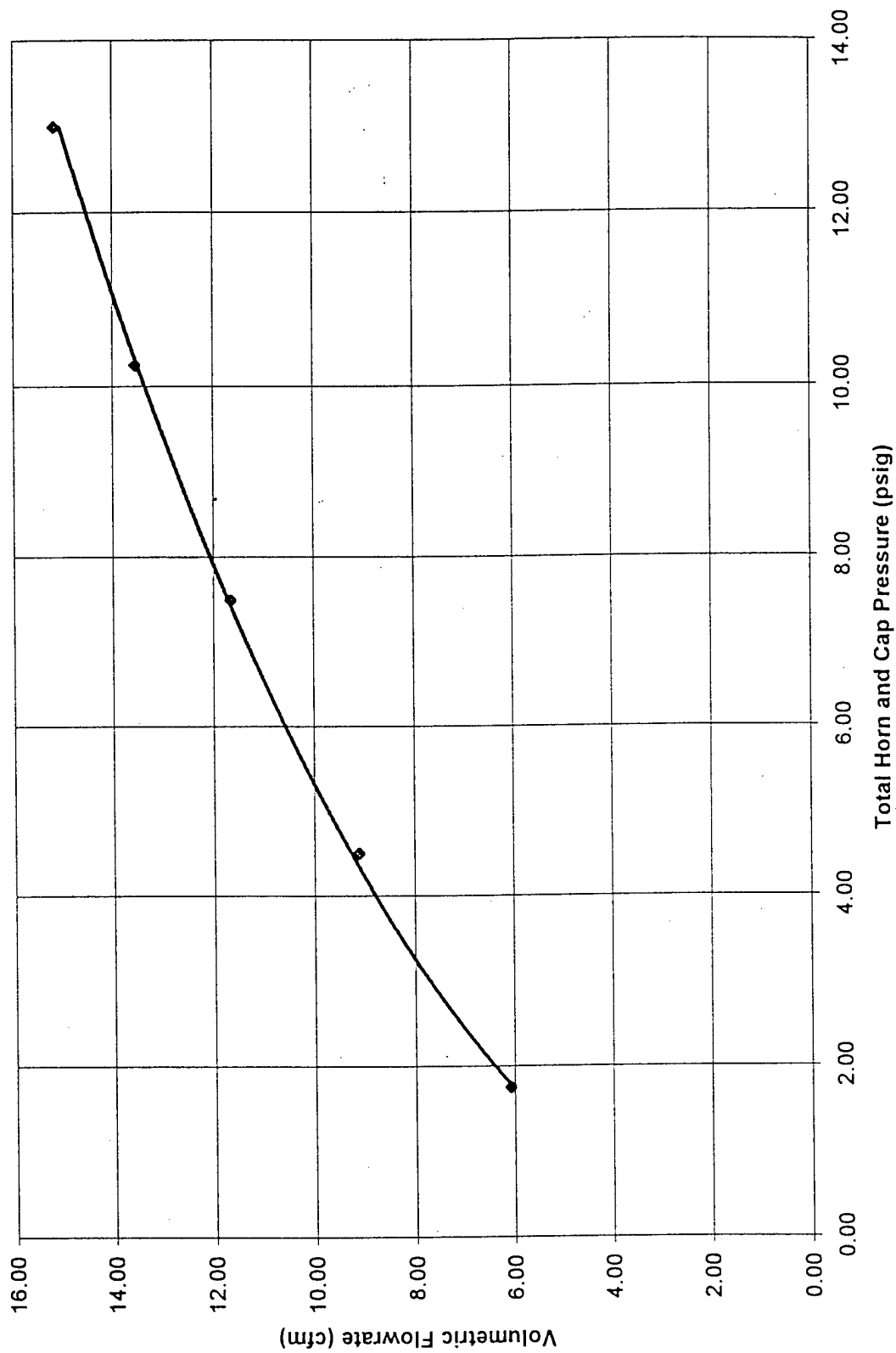


Figure A.5: Calibration of the DeVilbiss HVL P Spray Gun Volumetric Air Flowrate based on Total Horn and Cap Pressure

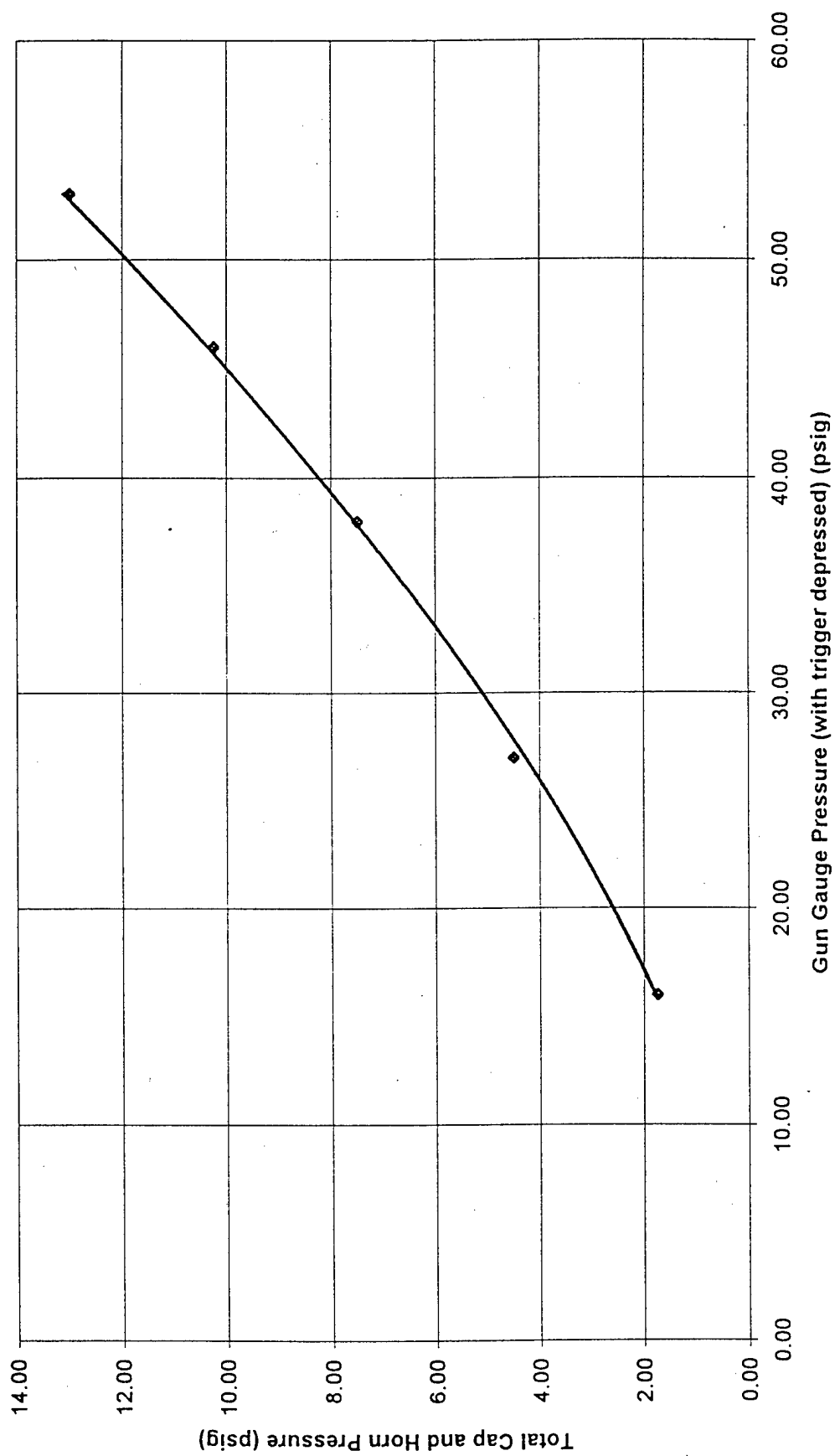


Figure A.6: Calibration of DeVilbiss HVL P Spray Gun Total Cap and Horn Pressure based on Gun Gauge Pressure

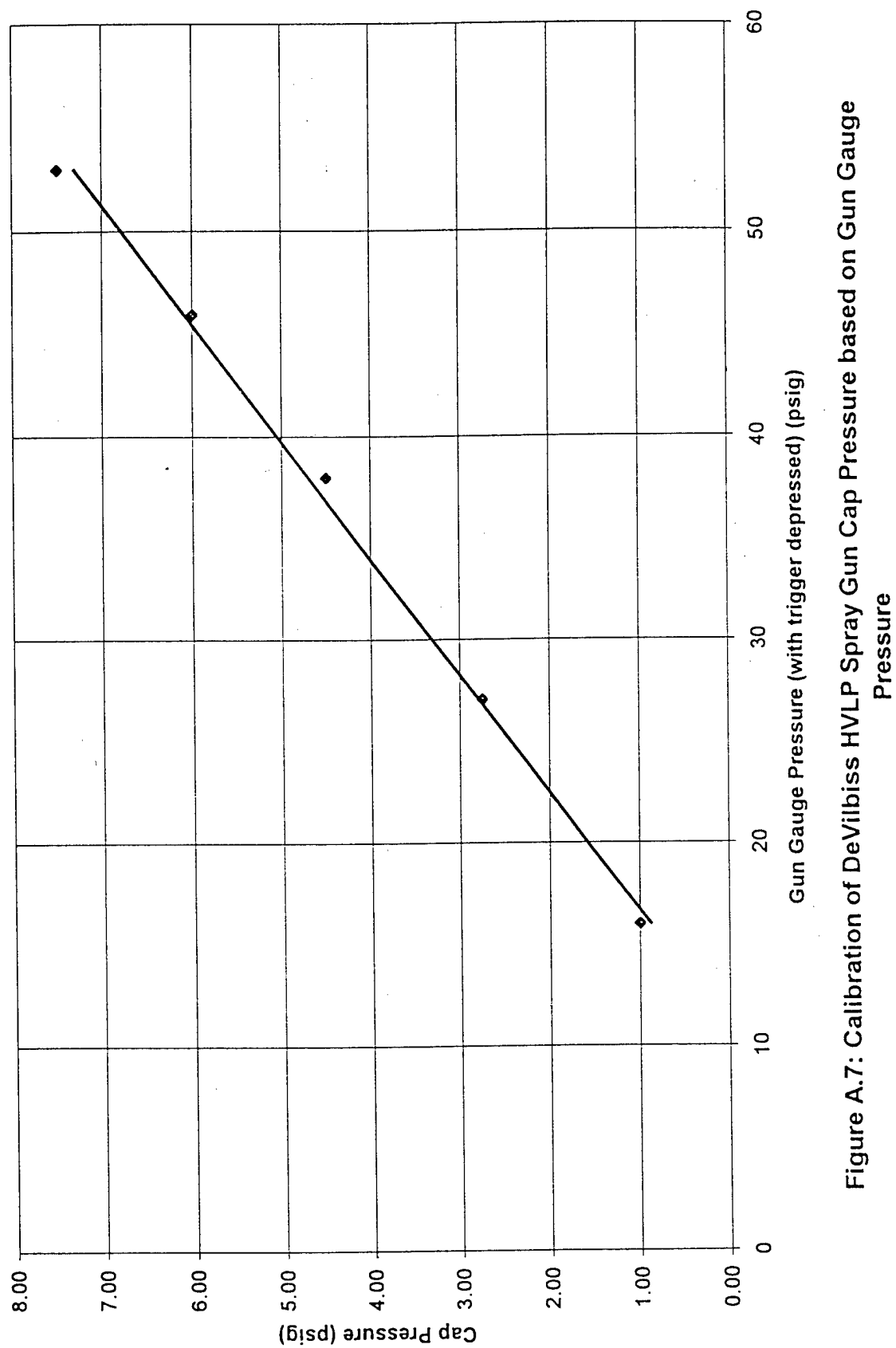


Figure A.7: Calibration of DeVilbiss HVLP Spray Gun Cap Pressure based on Gun Gauge

Pressure

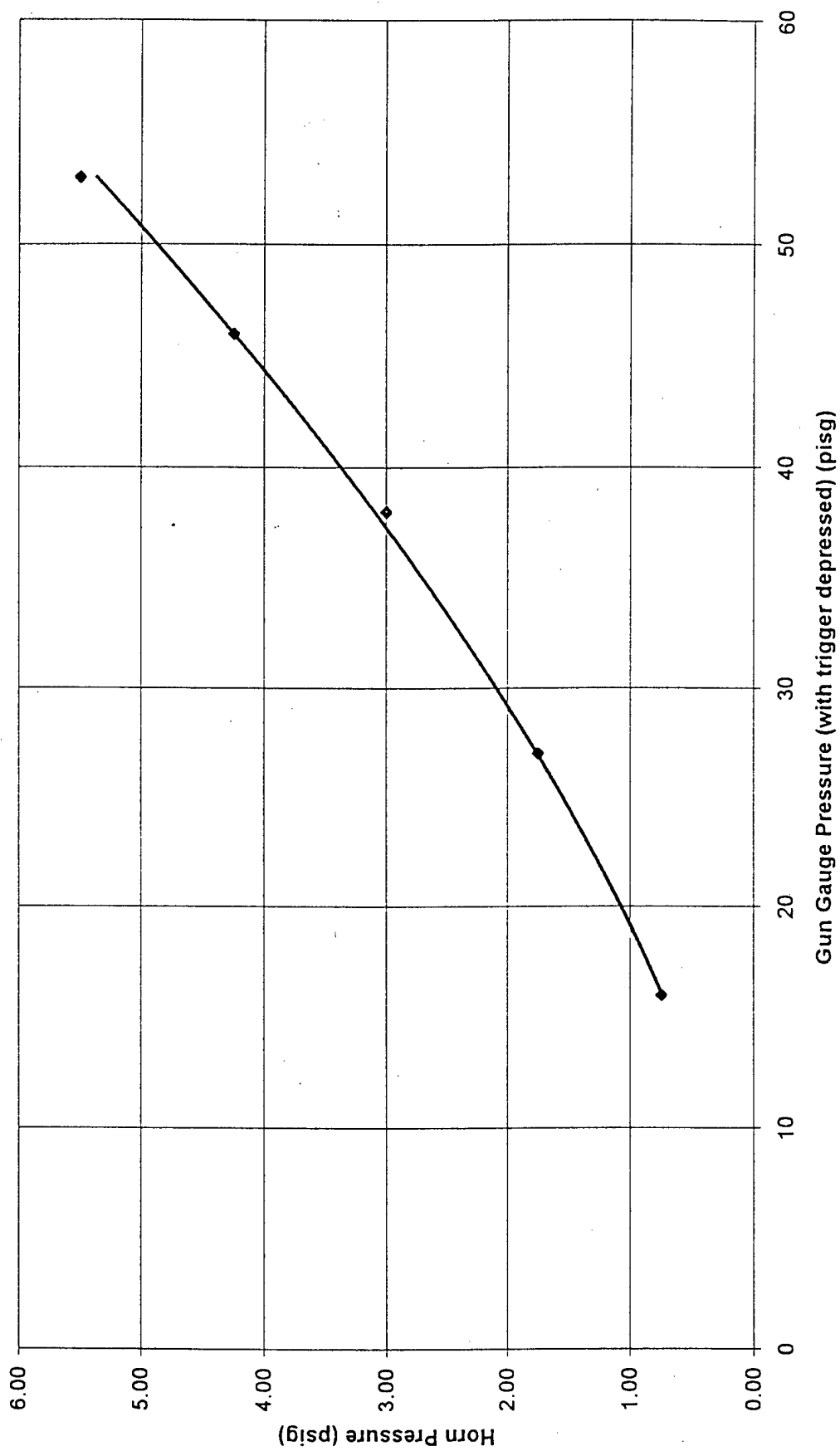


Figure A.8: Calibration of DeVilbiss Spray Gun Horn Pressure based on Gun Gauge Pressure

Table A.4: Calibration of HVLP Spray Gun Volumetric Airflow versus Gun Gauge Pressure Setting and Cap and Horn Pressure

The air cap of the HVLP was inserted into a plastic tube which led to a calibrated spirometer. Gun gauge pressure was achieved with the spray gun trigger depressed. 31 Jul 97, Bait Bay

Gun Gauge Pressure (trigger depressed) (psig)	Cap Pressure (psig)	Horn Pressure (psig)	Total Cap and Horn (psig)	Distance displaced by spirometer (mm)	Volume displaced (cc)	Time (seconds)	Time (minutes)	Volumetric Flowrate (cc/min)	Volumetric Flowrate (cfm)
16	1.00	0.75	1.75	600	79920	27.80	0.46	172489.21	6.09
16	1.00	0.75	1.75	600	79920	27.84	0.46	172241.38	6.08
16	1.00	0.75	1.75	600	79920	27.84	0.46	172241.38	6.08
16	1.00	0.75	1.75	600	79920	27.90	0.47	171870.97	6.07
Average Volumetric Flowrate									
27	2.75	1.75	4.50	600	79920	18.53	0.31	258780.36	9.14
27	2.75	1.75	4.50	600	79920	18.54	0.31	258640.78	9.13
27	2.75	1.75	4.50	600	79920	18.53	0.31	258780.36	9.14
27	2.75	1.75	4.50	600	79920	18.66	0.31	256977.49	9.08
Average Volumetric Flowrate									
38	4.50	3.00	7.50	600	79920	14.55	0.24	329567.01	11.64
38	4.50	3.00	7.50	600	79920	14.47	0.24	331389.08	11.70
38	4.50	3.00	7.50	600	79920	14.48	0.24	331160.22	11.69
38	4.50	3.00	7.50	600	79920	14.54	0.24	329793.67	11.65
Average Volumetric Flowrate									
46	6.00	4.25	10.25	600	79920	12.47	0.21	384538.89	13.58
46	6.00	4.25	10.25	600	79920	12.47	0.21	384538.89	13.58
46	6.00	4.25	10.25	600	79920	12.54	0.21	382392.34	13.50
46	6.00	4.25	10.25	600	79920	12.50	0.21	383616.00	13.55
Average Volumetric Flowrate									
53	7.50	5.50	13.00	600	79920	11.16	0.19	429677.42	15.17
53	7.50	5.50	13.00	600	79920	11.15	0.19	430062.78	15.19
53	7.50	5.50	13.00	600	79920	11.15	0.19	430062.78	15.19
53	7.50	5.50	13.00	600	79920	11.17	0.19	429292.75	15.16
Average Volumetric Flowrate									
									15.18

Table A.5: Calibration of the Rosenau Building Paint Booth

Fan set to highest speed to avoid dual operating conditions. Measurements recorded below are based on calibration of thermoanemometer. Recorded value is the mode during a time period of 15 minutes.

28 Jul 97, 1630-1700 hrs

64.2	121.1	136.5	130.7
48.7	109.5	132.7	120.1
48.7	111.4	129.8	113.4
55.5	98.9	137.5	126.9
217.1	440.9	536.5	491.1

Average velocity of paint booth 105.4 fpm  
 Average overall air flowrate 4773.7 cfm  
 Average flowrate 3 columns near cinder 122.4  
 1.16 greater for 3 columns near the cinder  
 Average flowrate 3 columns near flange 99.5  
 0.94 less than average for 3 columns near flange

1.23 ratio of 3 columns  
 near cinder to 3  
 columns near flange

29 Jul 97, 1100-1345 hrs

75.8	139.4	145.2	124.9
62.2	124.9	148.1	123.0
46.8	118.2	133.6	122.1
29.5	75.8	137.5	121.1
214.3	458.3	564.4	491.1

Average velocity of paint booth 108.0 fpm  
 Average air flowrate 4894.0 cfm  
 Average flowrate 3 columns near cinder 126.2  
 1.17 greater for 3 columns near the cinder  
 Average flowrate 3 columns near flange 103.1  
 0.95 less than average for 3 columns near flange

1.22 ratio of 3 columns  
 near cinder to 3  
 columns near flange

Fan set at moderate speed. Measurements recorded below are based on calibration of thermoanemometer.  
 Recorded value is the mode during a time period of 15 minutes.

15 Aug 97, 1500 hrs

44.9	97.0	121.1	105.7
46.8	96.0	124.0	111.4
46.8	88.3	115.3	114.3
74.8	97.9	102.8	109.5
213.3	379.2	463.2	440.9

Average velocity of paint booth 93.5 fpm  
 Average air flowrate 4238.4 cfm  
 Average flowrate 3 columns near cinder 106.9  
 1.14 greater for 3 columns near the cinder  
 Average flowrate 3 columns near flange 87.975  
 0.94 less for 3 columns near the flange

1.22 ratio of 3 columns  
 near cinder to 3  
 columns near flange

Table A.5: Calibration of the Rosenau Building Paint Booth (con't)

Fan set to lowest speed to avoid dual operating conditions. Measurements recorded below are based on calibration of thermoanemometer. Recorded value is the mode during a time period of 15 minutes.

8-Aug-97				Average velocity of paint booth		63.5 fpm	
				Average air flowrate		2875.1 cfm	
				Average flowrate 3 columns near cinder		74.3	
				1.17 greater for 3 columns near the cinder			
				Average flowrate 3 columns near flange		62.2	
				0.98 less for 3 columns near the flange			
						1.20 ratio of 3 columns near cinder to 3 columns near flange	
123.6				301.1		321.3	
						269.2	

10-Aug-97 Post experiment spot check of paint booth air flow.

Average velocity of paint booth				69.0 fpm	
Average air flowrate				3126.6 cfm	
n/a		86.4	n/a	n/a	
n/a		76.7	n/a	n/a	
n/a		50.7	n/a	n/a	
n/a		62.2	n/a	n/a	

9-Jan-98				Average velocity of paint booth		44.7 fpm	
				Average air flowrate		2024.3 cfm	
				Average flowrate 3 columns near cinder		46.9	
				1.05 greater for 3 columns near the cinder			
				Average flowrate 3 columns near flange		41.7	
				0.93 less for 3 columns near the flange			
						1.12 ratio of 3 columns near cinder to 3 columns near flange	
44				85.4		72.9	
40				36.2		66.1	
34.3				20.8		24.6	
34.3				17.9		23.7	
152.6				160.3		187.3	
						214.6	

Table A.5: Calibration of the Rosenau Building Paint Booth (con't)

28-Feb-98

55.5	68	100	n/a
48.7	68	93	n/a
60.3	62.2	68	n/a
52.6	54.5	60.3	n/a

Average velocity of paint booth 1  
Average air flowrate  
Est Average flow for 16 pt measu  
Est flow 3 columns near cinder w

65.9 fpm  
2987.2 cfm  
69.4  
80.4

1.22 ratio of 3 columns  
near cinder to 3  
columns near flang

11-Mar-98 Check of paint booth since 28 Feb 98.

50.7	64.2	84.4	n/a
49.7	59.4	81.5	n/a
57.4	67.1	65.1	n/a
72.9	37.2	56.5	n/a

Average velocity of paint booth 1  
Average air flowrate  
Est Average flow for 16 pt measu  
Est flow 3 columns near cinder w

62.2 fpm  
2817.3 cfm  
65.4  
75.9

Note: For the last two wind tunnel measurements, only 12 points were measured due to time constraints. Normal 16 point measure takes 4 hours to complete and a 12 point takes 2 hours.

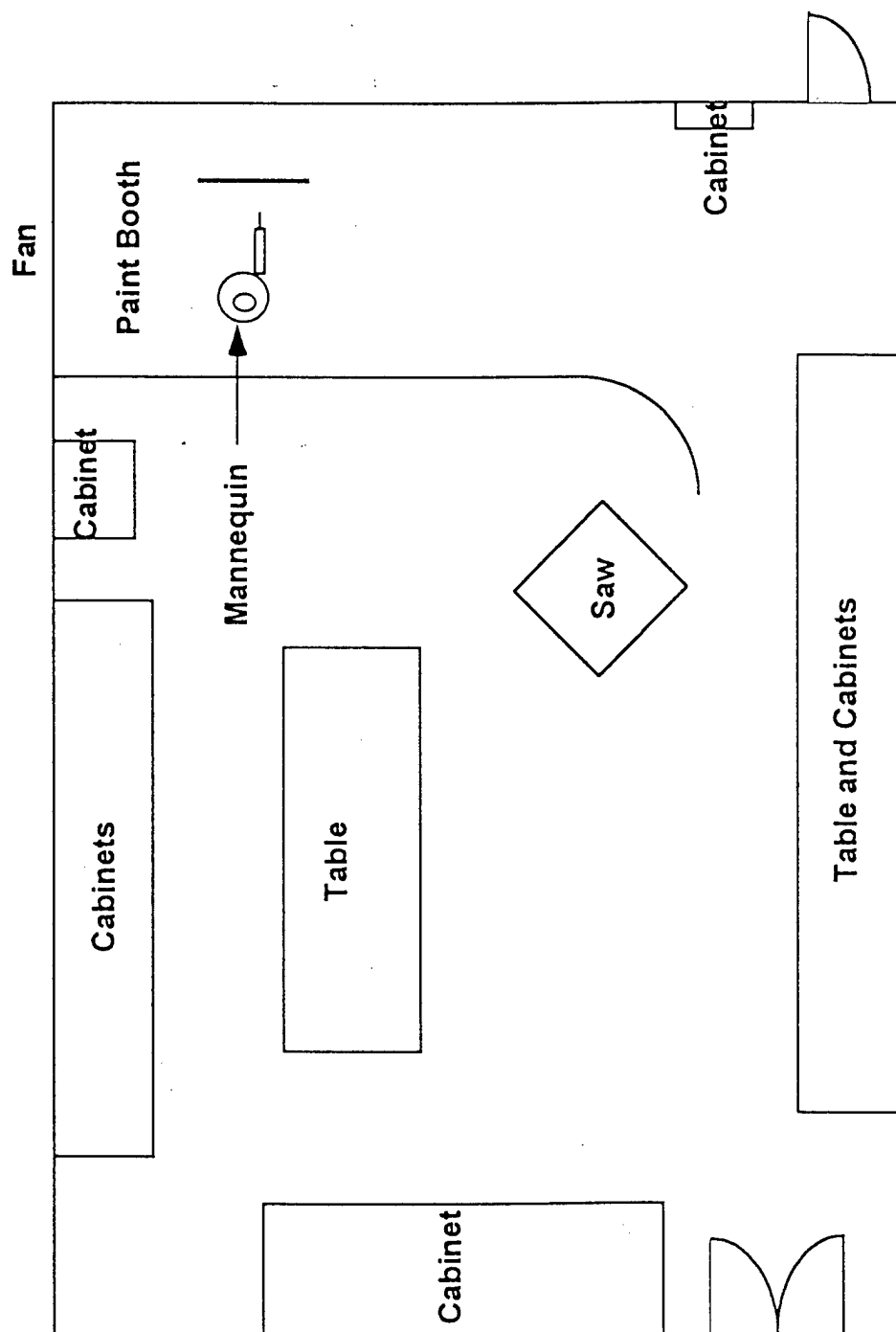


Figure A.9.: Schematic of Workroom Obstacles- Mannequin Oriented in 90-degree Position

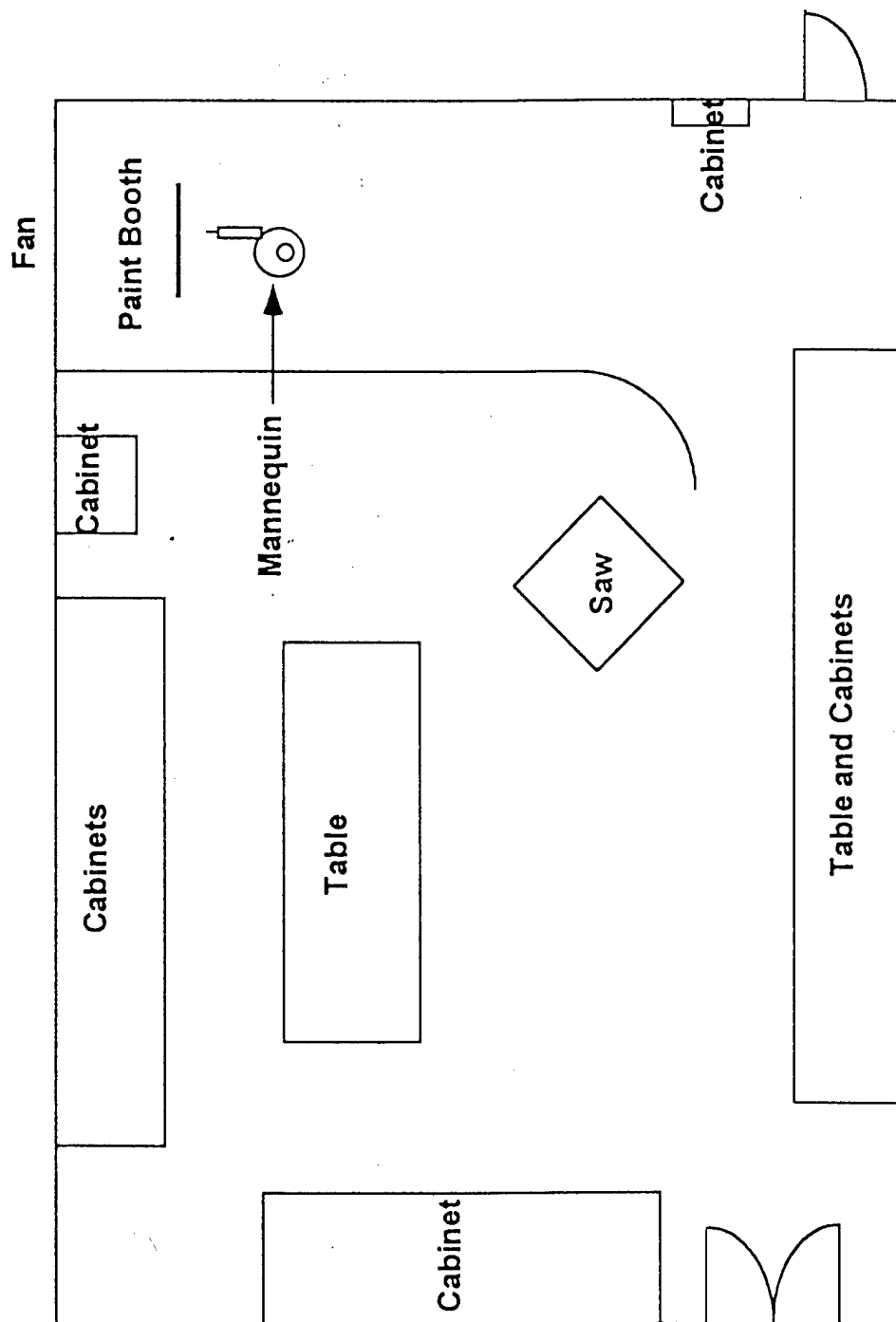


Figure A.10.: Schematic of Workroom Obstacles - Mannequin Oriented in 180-degree Position

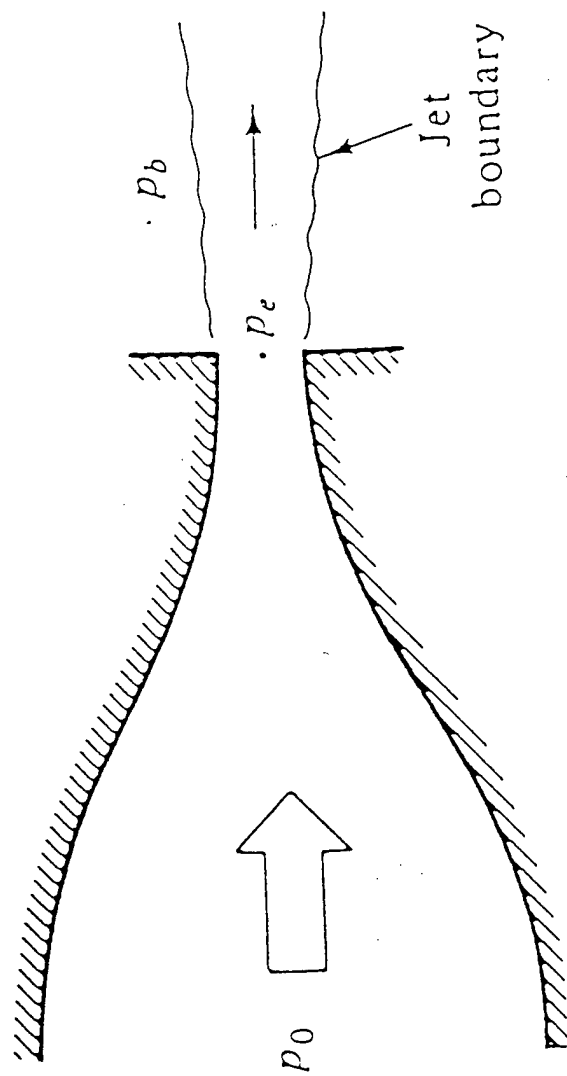


Figure A.11.: Converging Nozzle Diagram<sup>(8)</sup>

## APPENDIX B. Sample Calculations

The data for the calculations presented here are found in Tables A.6, A.7, and A.8. Refer to run number 1, 28 Feb 1998. Carlton's data was converted in a similar manner to momentum flux ratio.

### B.1 Oil Spray Rate

$$m_1 = \frac{\text{mass container (before)} - \text{mass container (after)}}{\text{sampling time}}$$

$$= \frac{(4091 - 958.9) \text{ g}}{30 \text{ min}} = 104.4 \text{ g/min}$$

### B.2 Oil Transfer Rate

$$m_{\text{transferred}} = \frac{\text{mass trough (before)} - \text{mass trough (after)}}{\text{sampling time}}$$

$$= \frac{(3414.7 - 706.7) \text{ g}}{30 \text{ min}} = 90.3 \text{ g/min}$$

### B.3 Overspray Rate

$$m_o = m_1 - m_{\text{transferred}}$$

$$= (104.4 - 90.3) \text{ g/min} = 14.1 \text{ g/min}$$

#### B.4. Dimensionless Concentration, CHUD/ $m_o$

Obtain freestream velocity (U) from Table A.5.

$$\frac{\text{CHUD}}{m_o} = \frac{(2.128 \text{ mg/m}^3) (6.17 \text{ ft}) (69.4 \text{ ft/min}) (1.17 \text{ ft}) (1 \text{ g}) (1 \text{ m}^3)}{(14.1 \text{ g/min}) (35.3145 \text{ ft}^3) (1000 \text{ mg})}$$
$$= 0.00213$$

#### B.5 Momentum Flux, $F_g/F_m$ (HVLP spray gun)

$$F_g = \rho_n A_n V_n^2 = m_n V_n$$

$$m_n = \rho_a Q = (0.075 \text{ lbm/ft}^3) (9.12 \text{ ft}^3/\text{min}) = 0.684 \text{ lbm/min}$$

$$F_g = 25069 \text{ (From Table A.6)}$$

$$F_m = \rho_a H D U^2$$

$$= (0.075 \text{ lbm/ft}^3) (6.17 \text{ ft}) (1.17 \text{ ft}) (69.4 \text{ ft/min})^2$$

$$= 2608$$

$$F_g/F_m = 9.61$$

Table A.6 HVLP Nozzle Velocity and Fg Calculation

gun	cap	horn	total	ma	Vn(cap)	Vn(horns)	K(total)	Fg
guag	press	pres	press	total	m/s	m/s	m <sup>4</sup> /s <sup>2</sup>	lbmft/min <sup>2</sup>
27	2.7866	1.76546	4.55206	0.6992902	202.0182	162.5893	0.801435	25069
32	3.6546	2.3379031	5.9925031	0.7928873	230.1022	186.6017	1.037141	32442
37	4.5226	2.9720153	7.4946153	0.8782036	254.3672	209.4744	1.276552	39931
38	4.6962	3.1059601	7.8021601	0.8944894	258.854	213.9178	1.324824	41441
42	5.3906	3.6647527	9.0553527	0.9574857	275.7723	231.2698	1.519072	47517
46	6.085	4.2594379	10.344438	1.0175173	291.2493	247.9696	1.714995	53646
47	6.2586	4.4135835	10.672184	1.0321223	294.92	252.0459	1.764212	55185
53	7.3002	5.3832135	12.683414	1.1168396	315.4898	275.7082	2.061263	64477

Table A.7 Overspray and Transfer Efficiency

180 degree Date	Run #	Uf				ml				m0			
		Freestrea fpm	Gun Gage psig	run time min	Bucket weight--gm		Trough weight--gm		OilSpraye gm/min	Oil Trans gm/min	Overspray gm/min	Transfer Efficiency	
					Before	After	Before	After					
10-Jan-98	1	44.7	27	30	4253.0	2129.2	821.9	2599.8	70.8	59.3	11.5	0.84	
10-Jan-98	2	44.7	38	30	4148.0	2067.7	754.4	2348.3	69.3	53.1	16.2	0.77	
10-Jan-98	3	44.7	53	30	4198.0	1925.9	756.0	2396.8	75.7	54.7	21.0	0.72	
10-Jan-98	4	44.7	46	30	4128.0	1814.3	795.3	2513.1	77.1	57.3	19.9	0.74	
10-Jan-98	5	44.7	27	30	4175.0	2104.0	750.7	2465.6	69.0	57.2	11.9	0.83	
10-Jan-98	6	44.7	38	30	4216.0	2105.1	788.2	2409.7	70.4	54.1	16.3	0.77	
10-Jan-98	7	44.7	46	30	4270.0	1992.7	734.0	2431.3	75.9	56.6	19.3	0.75	
11-Jan-98	9	44.7	27	30	4340.0	2133.7	734.0	2578.6	73.5	61.5	12.1	0.84	
11-Jan-98	10	44.7	53	30	4208.0	1751.2	728.7	2505.9	81.9	59.2	22.7	0.72	
11-Jan-98	11	44.7	38	30	4048.0	1937.3	730.7	2338.3	70.4	53.6	16.8	0.76	
11-Jan-98	12	44.7	46	30	4058.0	1704.6	728.4	2473.3	78.4	58.2	20.3	0.74	
11-Jan-98	14	44.7	46	30	4190.0	1706.0	728.2	2583.2	82.8	61.8	21.0	0.75	
11-Jan-98	15	44.7	38	30	4240.0	1793.0	741.1	2653.4	81.6	63.7	17.8	0.78	
11-Jan-98	16	44.7	27	30	4498.0	2199.3	729.0	2648.4	76.6	64.0	12.6	0.83	
28-Feb-98	1	69.4	27	30	4091	958.9	706.7	3414.7	104.4	90.3	14.1	0.86	
28-Feb-98	2	69.4	32	30	4485	1279.5	758.4	3475.2	106.9	90.6	16.3	0.85	
28-Feb-98	3	69.4	37	30	4413	1137.7	757.2	3471.6	109.2	90.5	18.7	0.83	
28-Feb-98	4	69.4	42	30.3	4566	1388.6	728.7	3282.2	104.9	84.3	20.6	0.80	
28-Feb-98	5	69.4	47	30	4452	1173.1	733.5	3286.3	109.3	85.1	24.2	0.78	
28-Feb-98	6	69.4	27	30	4516	1330	728.3	3468.3	106.2	91.3	14.9	0.86	
28-Feb-98	7	69.4	32	30	4479	1311.1	734.7	3397.1	105.6	88.7	16.9	0.84	
28-Feb-98	8	69.4	37	30	4444	1315.2	732	3310.8	104.3	86.0	18.3	0.82	
28-Feb-98	9	69.4	42	30	4513	1420.8	738.3	3237	103.1	83.3	19.8	0.81	
28-Feb-98	10	69.4	47	30.3	4471	1228.2	730	3293.5	107.0	84.6	22.4	0.79	
1-Mar-98	11	69.4	27	30	4488	1218	729.5	3553.2	109.0	94.1	14.9	0.86	
1-Mar-98	12	69.4	32	30	4404	1235.7	727	3398.1	105.6	89.0	16.6	0.84	
1-Mar-98	13	69.4	37	30	4480	1160.9	731	3478.3	110.6	91.6	19.1	0.83	
1-Mar-98	14	69.4	42	30	4384	1087.5	733	3415.7	109.9	89.4	20.5	0.81	
1-Mar-98	15	69.4	47	30	4545	1245.5	732.3	3351	110.0	87.3	22.7	0.79	

Table A.7 Overspray and Transfer Efficiency (pg 2)

Date	Run #	Freestrea fpm	Gun Gage psig	run time min	Bucket weight--gm		Trough weight--gm		OilSpray gm/min		Oil Trans gm/min		Overspray gm/min		Transfer Efficiency
					Before	After	Before	After	Before	After	Before	After	Before	After	
12-Mar-98	1	69.4	27	30	4208	1566.4	732.2	2962.3	88.1		74.3		13.7		0.84
12-Mar-98	2	69.4	32	30	4182	1745.6	728	2704	81.2		65.9		15.3		0.81
12-Mar-98	3	69.4	37	30	4211	1816.8	729.6	2600	79.8		62.3		17.5		0.78
12-Mar-98	4	69.4	42	30	4223	1720.8	727.3	2621.5	83.4		63.1		20.3		0.76
12-Mar-98	5	69.4	47	30	4180	1820.8	730.2	2457.6	78.6		57.6		21.1		0.73

## 90 degree

13-Mar-98	1	80.4	27	30	4439	2269.6	1055	2860	72.3		60.2		12.1		0.83
13-Mar-98	2	80.4	32	30	4436	2234.2	728.2	2503.7	73.4		59.2		14.2		0.81
13-Mar-98	4	80.4	42	30	4266	2150.5	733.9	2377.5	70.5		54.8		15.7		0.78
14-Mar-98	6	80.4	27	30	4478	2115.8	1034	3007	78.7		65.8		13.0		0.84
14-Mar-98	7	80.4	32	30	4310	1928	729.4	2656.6	79.4		64.2		15.2		0.81
14-Mar-98	8	80.4	37	10	4039	3238.5	730.7	1359.8	80.1		62.9		17.1		0.79
14-Mar-98	9	80.4	42	10	3954.8	3211	726.5	1281	74.4		55.5		18.9		0.75
15-Mar-98	1	80.4	47	10	2933.8	2201.2	859.5	1401.2	73.3		54.2		19.1		0.74
15-Mar-98	2	80.4	27	30	4494	2732.4	722.2	2144.1	58.7		47.4		11.3		0.81
15-Mar-98	4	80.4	37	10	4288	3602.7	726.6	1250.3	68.5		52.4		16.2		0.76
15-Mar-98	5	80.4	42	10	3602.7	2855.2	1250.3	1811.7	74.8		56.1		18.6		0.75
15-Mar-98	6	80.4	47	10	2855.2	2129	1811.7	2343.3	72.6		53.2		19.5		0.73
15-Mar-98	7	80.4	37	10	4271	3586.8	729	1251.5	68.4		52.3		16.2		0.76
15-Mar-98	8	80.4	42	10	4005	3274.9	1251.5	1799.2	73.0		54.8		18.2		0.75
15-Mar-98	9	80.4	47	10	3274.9	2600.8	1799.2	2287.9	67.4		48.9		18.5		0.72
17-Mar-98	1	80.4	32	30	3819	1920.9	961	2457.4	63.3		49.9		13.4		0.79

Table A.8 Dimensionless Concentration

180 degree		Ur		H		D		C				
Date	Run #	Freestrea fpm	Gun Gage psig	Man Heig ft	Man Diam ft	Pump flow l/min	Vol samp m3	Weight of Filter--mg		Mass Coll mg	Air Conc mg/m3	CUfHD/m0
								Before	After			
10-Jan-98	1	44.7	27	6.17	1.17	1.9	0.0570	13.059	13.183	0.124	2.175	1.72E-03
10-Jan-98	2	44.7	38	6.17	1.17	1.9	0.0570	13.773	13.965	0.192	3.368	1.90E-03
10-Jan-98	3	44.7	53	6.17	1.17	1.9	0.0570	12.024	13.699	1.675	29.386	1.28E-02
10-Jan-98	4	44.7	46	6.17	1.17	1.9	0.0570	13.333	14.010	0.677	11.877	5.46E-03
10-Jan-98	5	44.7	27	6.17	1.17	1.9	0.0570	12.020	12.121	0.101	1.772	1.36E-03
10-Jan-98	6	44.7	38	6.17	1.17	1.9	0.0570	12.057	12.554	0.497	8.719	4.88E-03
10-Jan-98	7	44.7	46	6.17	1.17	1.9	0.0570	12.902	13.666	0.764	13.404	6.33E-03
10-Jan-98	blank							13.551	13.546	-0.005		
10-Jan-98	blank							12.330	12.327	-0.003		
10-Jan-98	blank							14.136	14.139	0.003		
11-Jan-98	9	44.7	27	6.17	1.17	1.9	0.0570	13.320	13.474	0.154	2.702	2.05E-03
11-Jan-98	10	44.7	53	6.17	1.17	1.9	0.0570	14.249	15.675	1.426	25.018	1.01E-02
11-Jan-98	11	44.7	38	6.17	1.17	1.9	0.0570	13.781	14.117	0.336	5.895	3.21E-03
11-Jan-98	12	44.7	46	6.17	1.17	1.9	0.0570	13.386	13.571	0.185	3.246	1.46E-03
11-Jan-98	14	44.7	46	6.17	1.17	2.0	0.0600	12.910	14.137	1.227	20.450	8.91E-03
11-Jan-98	15	44.7	38	6.17	1.17	2.0	0.0600	13.008	13.304	0.296	4.933	2.53E-03
11-Jan-98	16	44.7	27	6.17	1.17	2.0	0.0600	13.257	13.493	0.236	3.933	2.84E-03
11-Jan-98	blank							12.950	12.950	0.000		
11-Jan-98	blank							13.125	13.131	0.006		
11-Jan-98	blank							13.634	13.637	0.003		
28-Feb-98	1	69.4	27	6.17	1.17	1.9	0.0564	12.237	12.357	0.120	2.128	2.13E-03
28-Feb-98	2	69.4	32	6.17	1.17	1.9	0.0564	13.834	14.002	0.168	2.979	2.59E-03
28-Feb-98	3	69.4	37	6.17	1.17	1.9	0.0564	12.649	12.809	0.160	2.838	2.15E-03
28-Feb-98	4	69.4	42	6.17	1.17	1.9	0.0570	12.999	13.198	0.199	3.494	2.41E-03
28-Feb-98	5	69.4	47	6.17	1.17	1.9	0.0564	14.633	14.952	0.319	5.657	3.31E-03
28-Feb-98	6	69.4	27	6.17	1.17	1.9	0.0564	12.745	12.900	0.155	2.749	2.62E-03
28-Feb-98	7	69.4	32	6.17	1.17	1.9	0.0564	13.878	14.062	0.184	3.263	2.75E-03
28-Feb-98	8	69.4	37	6.17	1.17	1.9	0.0564	13.884	14.039	0.155	2.749	2.13E-03
28-Feb-98	9	69.4	42	6.17	1.17	1.9	0.0564	12.204	12.474	0.270	4.788	3.43E-03
28-Feb-98	10	69.4	47	6.17	1.17	1.9	0.0570	13.914	14.245	0.331	5.812	3.68E-03

Table A.8 Dimensionless Concentration (pg 2)

180 degree		Uf		H		D		C				
Date	Run #	Freestrea fpm	Gun Gage psig	Man Heig ft	Man Diam ft	Pump flow l/min	Vol samp m3	Weight of Filter--mg		Mass Coll mg	Air Conc mg/m3	CuHd/m
								Before	After			
1-Mar-98	11	69.4	27	6.17	1.17	1.9	0.0561	15.218	15.383	0.165	2.941	2.80E-03
1-Mar-98	12	69.4	32	6.17	1.17	1.9	0.0561	15.041	15.315	0.274	4.884	4.18E-03
1-Mar-98	13	69.4	37	6.17	1.17	1.9	0.0561	13.030	13.204	0.174	3.102	2.31E-03
1-Mar-98	14	69.4	42	6.17	1.17	1.9	0.0561	12.518	12.888	0.370	6.596	4.57E-03
1-Mar-98	15	69.4	47	6.17	1.17	1.9	0.0561	13.108	13.585	0.477	8.503	5.31E-03
1-Mar-98	blank							15.291	15.300	0.009		
1-Mar-98	blank							12.523	12.529	0.006		
1-Mar-98	blank							14.784	14.783	-0.001		
1-Mar-98	blank							12.358	12.358	0.000		
1-Mar-98	blank							13.784	13.791	0.007		
12-Mar-98	1	69.4	27	6.17	1.17	1.9	0.0582	14.783	14.871	0.088	1.513	1.56E-03
12-Mar-98	2	69.4	32	6.17	1.17	1.9	0.0582	15.169	15.276	0.107	1.839	1.70E-03
12-Mar-98	3	69.4	37	6.17	1.17	1.9	0.0582	15.115	15.295	0.180	3.094	2.51E-03
12-Mar-98	4	69.4	42	6.17	1.17	1.9	0.0582	14.837	15.002	0.165	2.836	1.98E-03
12-Mar-98	5	69.4	47	6.17	1.17	1.9	0.0582	14.664	15.314	0.650	11.172	7.52E-03
12-Mar-98	blank							14.474	14.477	0.003		
12-Mar-98	blank							13.888	13.892	0.004		
12-Mar-98	blank							14.674	14.673	-0.001		
90 degree												
13-Mar-98	1	80.4	27	6.17	1.17	1.9	0.0582	14.848	14.988	0.140	2.406	3.25E-03
13-Mar-98	2	80.4	32	6.17	1.17	1.9	0.0582	14.754	15.983	1.229	21.124	2.44E-02
13-Mar-98	4	80.4	42	6.17	1.17	1.9	0.0582	14.385	16.161	1.776	30.526	3.19E-02
14-Mar-98	6	80.4	27	6.17	1.17	1.9	0.0582	13.888	14.205	0.317	5.449	6.90E-03
14-Mar-98	7	80.4	32	6.17	1.17	1.9	0.0582	14.066	15.424	1.358	23.342	2.53E-02
14-Mar-98	8	80.4	37	6.17	1.17	1.9	0.0194	15.700	16.621	0.921	47.491	4.55E-02
14-Mar-98	9	80.4	42	6.17	1.17	1.9	0.0194	15.046	15.983	0.937	48.316	4.19E-02
14-Mar-98	blank							15.065	15.066	0.001		
14-Mar-98	blank							14.496	14.498	0.002		

Table A. 8 Dimensionless Concentration (pg 3)

90 degree		Uf		H		D		C				
Date	Run #	Freestrea fpm	Gun Gage psig	Man Heig ft	Man Diam ft	Pump flow l/min	Vol samp m3	Weight of Filter--mg		Mass Coll mg	Air Conc mg/m3	CUfHD/m
14-Mar-98	blank							Before	After	0.008		
14-Mar-98	blank							15.250	15.258			
								16.058	16.062	0.004		
15-Mar-98	1	80.4	47	6.17	1.17	1.9	0.0188	15.924	17.480	1.556	82.603	7.11E-02
15-Mar-98	2	80.4	27	6.17	1.17	1.9	0.0565	15.831	17.604	1.773	31.374	4.55E-02
15-Mar-98	4	80.4	37	6.17	1.17	1.9	0.0188	15.808	16.430	0.622	33.020	3.36E-02
15-Mar-98	5	80.4	42	6.17	1.17	1.9	0.0188	15.664	17.193	1.529	81.170	7.16E-02
15-Mar-98	6	80.4	47	6.17	1.17	1.9	0.0188	15.724	17.563	1.839	97.627	8.24E-02
15-Mar-98	7	80.4	37	6.17	1.17	1.9	0.0188	15.222	16.235	1.013	53.777	5.46E-02
15-Mar-98	8	80.4	42	6.17	1.17	1.9	0.0188	15.429	17.042	1.613	85.629	7.71E-02
15-Mar-98	9	80.4	47	6.17	1.17	1.9	0.0188	15.454	17.252	1.798	95.450	8.46E-02
15-Mar-98	blank							15.439	15.439	0.000		
15-Mar-98	blank							15.731	15.734	0.003		
15-Mar-98	blank							15.755	15.755	0.000		
15-Mar-98	blank							15.835	15.832	-0.003		
15-Mar-98	blank							15.153	15.148	-0.005		
17-Mar-98	1	80.4	32	6.17	1.17	1.9	0.0565	16.150	17.577	1.427	25.252	3.10E-02
17-Mar-98	blank							16.415	16.422	0.007		
17-Mar-98	blank							16.613	16.636	0.023		

Table A.9 Momentum Flux Ratio

180 degree		Uf		H		D		
Date	Run #	Freestrea fpm	Gun Gage psig	Man Heig ft	Man Diam ft	Fg	Fm	Fg/Fm
10-Jan-98	1	44.7	27	6.17	1.17	25069	1082	23.17
10-Jan-98	2	44.7	38	6.17	1.17	41441	1082	38.31
10-Jan-98	3	44.7	53	6.17	1.17	64477	1082	59.60
10-Jan-98	4	44.7	46	6.17	1.17	53646	1082	49.59
10-Jan-98	5	44.7	27	6.17	1.17	25069	1082	23.17
10-Jan-98	6	44.7	38	6.17	1.17	41441	1082	38.31
10-Jan-98	7	44.7	46	6.17	1.17	53646	1082	49.59
11-Jan-98	9	44.7	27	6.17	1.17	25069	1082	23.17
11-Jan-98	10	44.7	53	6.17	1.17	64477	1082	59.60
11-Jan-98	11	44.7	38	6.17	1.17	41441	1082	38.31
11-Jan-98	12	44.7	46	6.17	1.17	53646	1082	49.59
11-Jan-98	14	44.7	46	6.17	1.17	53646	1082	49.59
11-Jan-98	15	44.7	38	6.17	1.17	41441	1082	38.31
11-Jan-98	16	44.7	27	6.17	1.17	25069	1082	23.17
28-Feb-98	1	69.4	27	6.17	1.17	25069	2608	9.61
28-Feb-98	2	69.4	32	6.17	1.17	32442	2608	12.44
28-Feb-98	3	69.4	37	6.17	1.17	39931	2608	15.31
28-Feb-98	4	69.4	42	6.17	1.17	47517	2608	18.22
28-Feb-98	5	69.4	47	6.17	1.17	55185	2608	21.16
28-Feb-98	6	69.4	27	6.17	1.17	25069	2608	9.61
28-Feb-98	7	69.4	32	6.17	1.17	32442	2608	12.44
28-Feb-98	8	69.4	37	6.17	1.17	39931	2608	15.31
28-Feb-98	9	69.4	42	6.17	1.17	47517	2608	18.22
28-Feb-98	10	69.4	47	6.17	1.17	55185	2608	21.16
1-Mar-98	11	69.4	27	6.17	1.17	25069	2608	9.61
1-Mar-98	12	69.4	32	6.17	1.17	32442	2608	12.44
1-Mar-98	13	69.4	37	6.17	1.17	39931	2608	15.31
1-Mar-98	14	69.4	42	6.17	1.17	47517	2608	18.22
1-Mar-98	15	69.4	47	6.17	1.17	55185	2608	21.16

Table A.9 Momentum Flux Ratio (pg2)

180 degree		Uf	H		D			
Date	Run #	Freestrea fpm	Gun Gage psig	Man Heig ft	Man Diam ft	Fg	Fm	Fg/Fm
12-Mar-98	1	69.4	27	6.17	1.17	25069	2608	9.61
12-Mar-98	2	69.4	32	6.17	1.17	32442	2608	12.44
12-Mar-98	3	69.4	37	6.17	1.17	39931	2608	15.31
12-Mar-98	4	69.4	42	6.17	1.17	47517	2608	18.22
12-Mar-98	5	69.4	47	6.17	1.17	55185	2608	21.16

90 degree

13-Mar-98	1	80.4	27	6.17	1.17	25069	3500	7.16
13-Mar-98	2	80.4	32	6.17	1.17	32442	3500	9.27
13-Mar-98	4	80.4	42	6.17	1.17	47517	3500	13.58
14-Mar-98	6	80.4	27	6.17	1.17	25069	3500	7.16
14-Mar-98	7	80.4	32	6.17	1.17	32442	3500	9.27
14-Mar-98	8	80.4	37	6.17	1.17	39931	3500	11.41
14-Mar-98	9	80.4	42	6.17	1.17	47517	3500	13.58
15-Mar-98	1	80.4	47	6.17	1.17	55185	3500	15.77
15-Mar-98	2	80.4	27	6.17	1.17	25069	3500	7.16
15-Mar-98	4	80.4	37	6.17	1.17	39931	3500	11.41
15-Mar-98	5	80.4	42	6.17	1.17	47517	3500	13.58
15-Mar-98	6	80.4	47	6.17	1.17	55185	3500	15.77
15-Mar-98	7	80.4	37	6.17	1.17	39931	3500	11.41
15-Mar-98	8	80.4	42	6.17	1.17	47517	3500	13.58
15-Mar-98	9	80.4	47	6.17	1.17	55185	3500	15.77
17-Mar-98	1	80.4	32	6.17	1.17	32442	3500	9.27

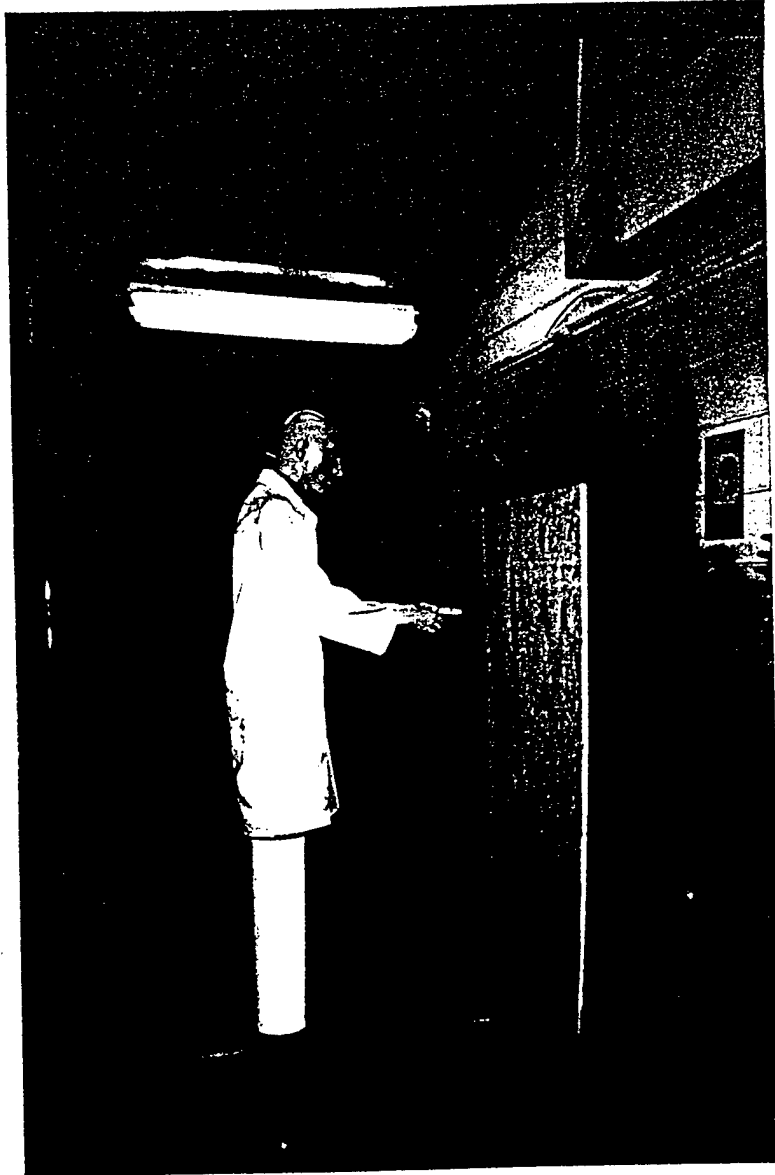


Figure A.12.: Mannequin at 90 Degree Orientation to the Freestream

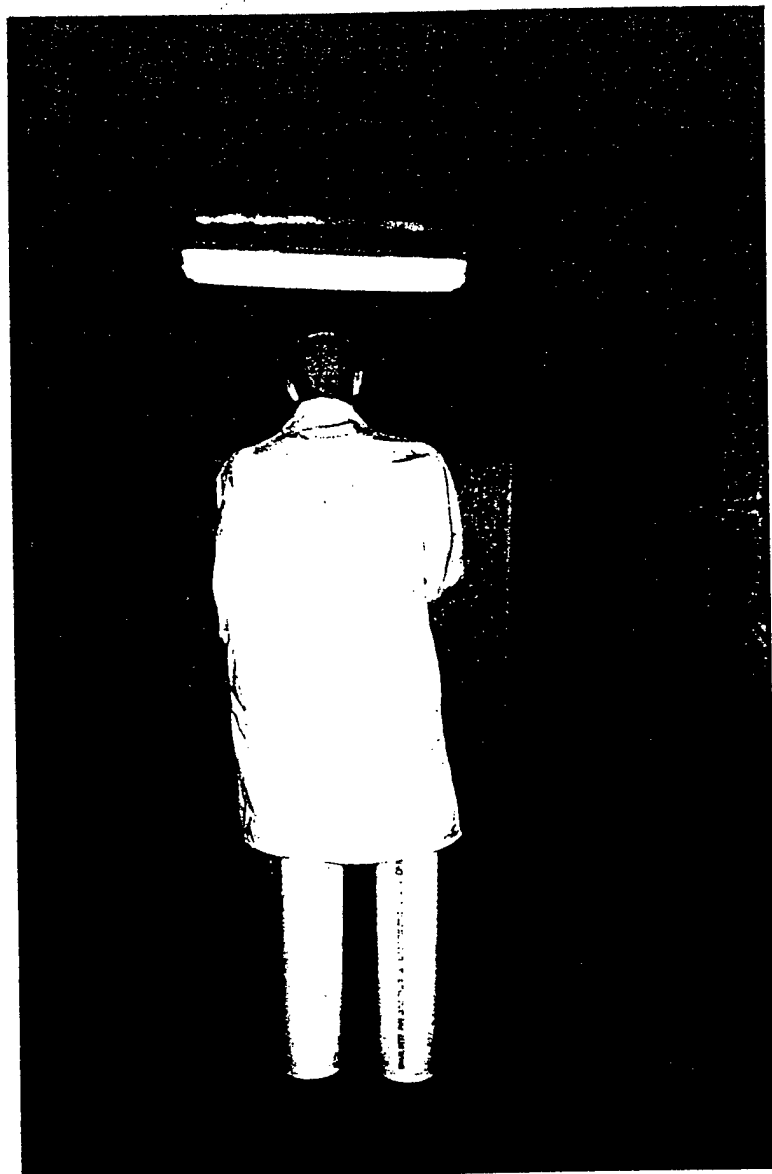


Figure A.13.: Mannequin at 180 Degree Orientation to the Freestream